Molecular Biology of the Cell
Vol. 19, 3080–3096, July 2008

The Sac1 Phosphoinositide Phosphatase Regulates Golgi Membrane Morphology and Mitotic Spindle Organization in Mammals

Yang Liu, Malika Boukhelifa, Emily Tribble, Elizabeth Morin-Kensicki, Andrea Uetrecht, James E. Bear, and Vytas A. Bankaitis

Department of Cell and Developmental Biology, Lineberger Comprehensive Cancer Center, University of North Carolina School of Medicine, Chapel Hill, NC 27599-7090

Submitted December 27, 2007; Revised April 1, 2008; Accepted May 1, 2008
Monitoring Editor: Adam Linstedt

Phosphoinositides (PIPs) are ubiquitous regulators of signal transduction events in eukaryotic cells. PIPs are degraded by various enzymes, including PIP phosphatases. The integral membrane Sac1 phosphatases represent a major class of such enzymes. The central role of lipid phosphatases in regulating PIP homeostasis notwithstanding, the biological functions of Sac1-phosphatases remain poorly characterized. Herein, we demonstrate that functional ablation of the single murine Sac1 results in preimplantation lethality in the mouse and that Sac1 insufficiencies result in disorganization of mammalian Golgi membranes and mitotic defects characterized by multiple mechanically active spindles. Complementation experiments demonstrate mutant mammalian Sac1 proteins individually defective in either phosphoinositide phosphatase activity, or in recycling of the enzyme from the Golgi system back to the endoplasmic reticulum, are nonfunctional proteins in vivo. The data indicate Sac1 executes an essential household function in mammals that involves organization of both Golgi membranes and mitotic spindles and that both enzymatic activity and endoplasmic reticulum localization are important Sac1 functional properties.

INTRODUCTION

Spatial and temporal regulation of intracellular signaling in eukaryotic cells involves the compartmentalization of membrane surfaces into discrete, albeit often transient, functional units. There are several biochemical strategies by which cells generate such units or domains. One well-established strategy uses the chemical diversity offered by phosphoinositides (PIPs), i.e., phosphorylated forms of phosphatidylinositol (PtdIns) (Majerus, 1997; Fruman *et al*., 1998; Strahl and Thorner, 2007). The chemical heterogeneity of individual PIP species permits the construction of chemically unique platforms on membrane surfaces that, in turn, recruit unique cohorts of proteins that drive specific biological reactions. Spatial and temporal control of such reactions requires a finely coordinated balance between the activities of the lipid kinases that produce PIPs and the activities of enzymes that degrade them. PIP turnover is catalyzed by two general classes of enzymes: phospholipases and PIP phosphatases. Although experimental scrutiny of the phospholipases has historically been more intense, recent demonstrations of the significant biological functions played by PTEN, the myotubularins, and synaptojanins highlight the general importance of PIP phosphatases (Wishart *et al*., 2001; Wishart and Dixon, 2002; Wenk and De Camilli, 2004).

The SAC domain derives from the yeast Sac1 protein (ySac1; Cleves *et al*., 1989), and it represents a signature for PIP phosphatase catalytic activity (Guo *et al*., 1999). PIP phosphatases such as phosphatase and tensin homolog (mutated in multiple advanced cancers 1) (PTEN) (Maehama *et al*., 2001), synaptojanins (Cremona *et al*., 1999), and synaptojanin-like proteins (Srinivasan *et al*., 1997; Stolz *et al*., 1998) all harbor SAC domains. The prototypical member of this family, ySac1, catalyzes the dephosphorylation of PIPs with the intriguing exception that PtdIns-4,5-P_2 is not a substrate (Guo *et al*., 1999; Rivas *et al*., 1999; Hughes *et al*., 2000). In keeping with the multiplicity of PIP signaling functions in eukaryotes, Sac1 loss-of-function (LOF) elicits pleitotropic effects in yeast that reflect broad-ranging alterations in multiple aspects of lipid metabolism (Cleves *et al*., 1989; Novick *et al*., 1989; Rivas *et al*., 1999; Tahirovic *et al*., 2005). Such metabolic alterations contribute to mislocalization of PIP binding proteins from the Golgi complex to inappropriate compartments (Li *et al*., 2002). ySac1 is an unusual PIP phosphatase in several respects. First, ySac1 degrades a PtdIns-4-P pool produced by the Stt4 PtdIns 4-OH kinase, one of three PtdIns 4-OH kinases in this organism (Nemoto *et al*., 2000; Foti *et al*., 2001). Second, ySac1 is an integral membrane protein of endoplasmic reticulum (ER) and Golgi membranes (Cleves *et al*., 1989; Whitters *et al*., 1993; Nemoto *et al*., 2000). This disposition is determined by two C-terminal membrane anchor sequences with the large catalytic domain

This article was published online ahead of print in *MBC in Press* (http://www.molbiolcell.org/cgi/doi/10.1091/mbc.E07–12–1290) on May 14, 2008.

Address correspondence to: Vytas A. Bankaitis (vytas@med.unc.edu).

Abbreviations used: BrdU, bromodeoxyuridine; BSA, bovine serum albumin; ER, endoplasmic reticulum; ES, embryonic stem; FACS, fluorescence-activated cell sorting; GAG, glycosaminoglycan; GFP, green fluorescent protein; Ins, inositol; LOF, loss-of-function; MT, microtubule; PBS, phosphate-buffered saline; PIP, phosphoinositide; PITP, phosphatidylinositol transfer protein; PtdIns, phosphatidylinositol; RFP, red fluorescent protein; RT-PCR, reverse transcriptase-polymerase chain reaction; TGN, *trans*-Golgi network; VSV-G, vesicular stomatitis virus glycoprotein.

oriented toward the cytosolic face (Konrad *et al*., 2002; Supplemental Figure S1A). Finally, ER residence of ySac1 as an integral protein is key to ySac1 function in vivo (Rivas *et al*., 1999).

ySac1 homologues are conserved throughout the Eukaryota (Supplemental Figure S1B). Mammalian Sac1 is an integral membrane protein with an anchor-sequence arrangement similar to that of ySac1p (Supplemental Figure S1, A and B), and it primarily resides in ER membranes (Nemoto *et al*., 2000). ER retention of the mammalian enzyme is controlled by a COP1-Sac1 binding interaction that captures enzyme in the Golgi system and recycles it back to the ER in COP1 vesicles (Rohde *et al*., 2003). Herein, we report the consequences of loss of Sac1 function in mice and in human cell models. Sac1 nullizygosity results in preimplantation lethality in mice, and reduced hSac1 expression is deleterious to cell viability of human cell lines. From a subcellular perspective, specific derangements of Golgi membrane and mechanically active mitotic spindle organization are recorded in hSac1-depleted cells. Although cargo transport to, through, and from the disorganized Golgi system is not impaired, hSac1-depleted cells arrest in mitosis. The Golgi and mitotic spindle phenotypes are rescued by expression of silencing-resistant murine Sac 1 (mSac1), but not by "catalytic-dead" mSac1 or by mSac1 forms incompetent for COP1 binding. We conclude that mammalian Sac1 PIP phosphatases execute essential housekeeping functions required for proper Golgi and mitotic spindle organization and that both PIP phosphatase activity and COP1-dependent retrograde trafficking are functionally important properties of these enzymes.

MATERIALS AND METHODS

Bioinformatic Methods

Sequences were analyzed by BLAST (http://www.ncbi.nlm.nih.gov/BLAST/). Sequence alignments were generated by the MegAlign 5.05 program.

Media and Genetic Techniques

Lithium acetate yeast transformation and genetic techniques were performed, and yeast media were prepared as described previously (Kearns *et al*., 1997; Xie *et al*., 1998; Guo *et al*., 1999; Phillips *et al*., 1999). Yeast strains used in this study included: CTY182 (MATa *ura3-52 lys2-801 Δhis3-200*), CTY244 (CTY182 *sac1Δ1-354::HIS3*) (Cleves *et al*., 1991; Phillips *et al*., 1999).

Site-directed Mutagenesis

Site-directed mutagenesis of murine *SAC1* was performed as described previously (Nemoto *et al*., 2000). Mutagenic primers were as follows: for $msac1^{D391N}$, 5′-CGCAGCA ACTGCATGAATTGTCTAGACAG-3′ and 5′-CTGTCTAGACAATTCATGCAGTTGCTGCG-3′; for $msac1^{A442V}$, 5′-CCTGGGCCGATAATGTTAATGCTTGTGCC-3′ and 5′-GGCACAAGCATTAACA TTATCGGCCCAGG-3′; and for $msac1^{R480H}$, 5′-GGCTTCAACTCATTATTACACTATTACAAGAACA AC-3′ and 5′-GTTGTTCTTGTAATAGTGTAATAATGAGTTGAAGCC-3′. Fidelity of mutagenesis was confirmed by DNA sequence analysis. The point mutant *msac1* and wild-type *mSAC1* cDNAs were individually subcloned into a derivative of the yeast *URA3* episomal vector YEplac195, which is engineered to express genes of interest in yeast from the constitutive *SEC14* promoter.

Inositol Radiolabeling and PIP Analyses

PIPs were identified and quantified as described previously (Guo *et al*., 1999; Rivas *et al*., 1999; Nemoto *et al*., 2000). To analyze PIPs in mammalian cells, control and *hSAC1* small interfering RNA (siRNA)-treated HeLa cells were cultured in six-well plates, and radiolabeled to steady state with 100 μCi/ml [^{3}H]inositol (Ins) for 48 h. Cells were scraped, phospholipids (PLs) were extracted and deacylated with methylamine, and soluble glycerophosphoinositol species were resolved and quantified as described previously (Guo *et al*., 1999; Rivas *et al*., 1999; Nemoto *et al*., 2000; Alb *et al*., 2002).

Characterization of the msac1::β-GEO Splice-Trap Allele

To examine *SAC1* function in mice, we characterized a Bay Genomics embryonic stem (ES) cell line with a pGT1dTM splice-trap insertion annotated to reside in the first intron of the *mSAC1* gene (Figure 1A). The gene-trap contains a splice-acceptor sequence positioned upstream of a *β-GEO* reporter (β-galactosidase::neomycin phosphotransferase gene fusion). Gene trap insertion is expected to divert normal *mSAC1* splicing such that the first exon is fused to an otherwise promoter-less *β-GEO* gene. To confirm annotation of the splice-trap insertion site within the 12.4-kb *mSAC1* intron 1, the pGT1dTM splice-trap insertion site was first mapped to low resolution by Southern blotting. By taking advantage of a unique SphI site in pGT1dTM, and of the endogenous SphI and EcoNI sites in *mSAC1* intron 1, we determined the insertion lay within the proximal 2.9 kb of *mSAC1* intron 1 (Figure 1B and Supplemental Figure S2). The insertion site was mapped more precisely by

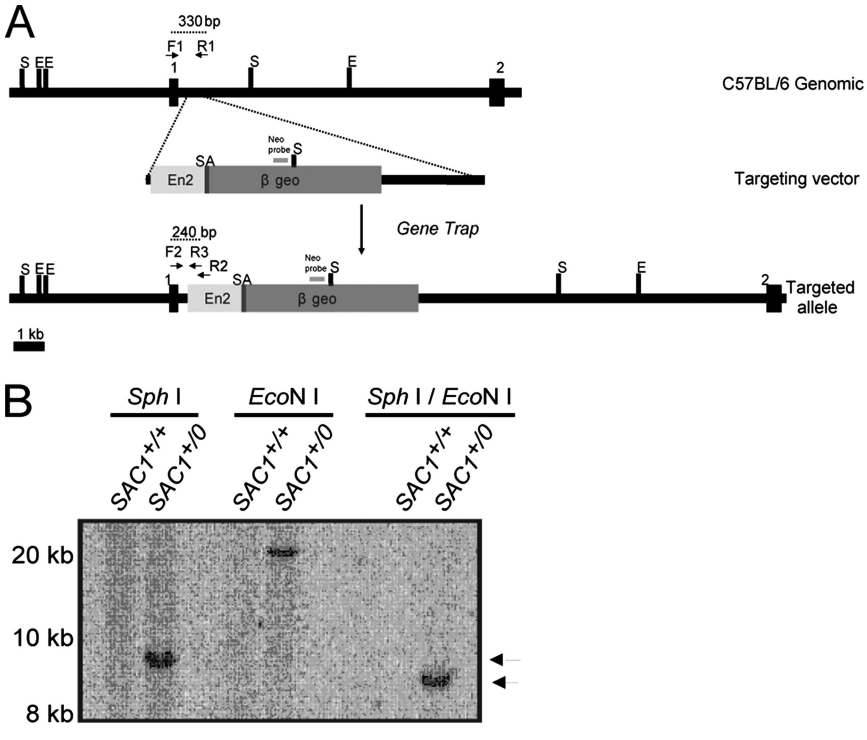

Figure 1. Genetic ablation of the mammalian *SAC1* gene. (A) *SAC1* insertion mutation. ES cells (NPX473) used to produce *SAC1*-deficient mice carried a gene trap insertion of pGT1dTM in the *SAC1* locus. A 0.3-kb fragment upstream of the vector SphI site, designated the Neo probe, was used as a diagnostic probe in Southern blots. The insertion site within *SAC1* intron 1 was determined by PCR. PCR primers: F1, 120bp@Intron1-F; F2, 310bp@Intron1-F; R1, 630bp@Intron1-R; R2,1730bp@pGTM-R; and R3, 1kb@pGTM-R (see Supplemental Table S1). Restriction sites: S, SphI; E, EcoNI. SA, splice acceptor. (B) Identification of gene-trap insertion by Southern blot. Genomic DNA from $SAC1^{+/+}$ and $SAC1^{+/0}$ ES cells was digested with SphI or EcoNI or both, transferred to nitrocellulose, and hybridized with radiolabeled Neo probe. Arrows at right indicate the fragment released from the double digestion was 0.5 kb smaller than that released by SphI digestion.

polymerase chain reaction (PCR) by using forward primers to walk down *mSAC1* intron 1 sequences. In those assays, a common reverse primer that hybridizes uniquely to pGT1dTM was used (Figure 1A). A 1.1-kb product was amplified using forward primer F1: 120bp@Intron1-F, which anneals 120 bp downstream of the 5′ end of the intron 1, and reverse primer R2: 1730bp@pGTM-R (Supplemental Table S1). This result was corroborated using forward primer F2: 310bp@Intron1-F (anneals 310 base pairs downstream of the 5′ end of intron 1) in combination with reverse primer R3: 1kb@pGTM-R (anneals 1 kb downstream of the 5′ end of vector; Supplemental Table S1). Nucleotide sequences of these PCR products mapped the pGT1dTM insertion site 400 bp downstream of the 3′ end of *mSAC1* exon 1. Although we found rearrangements at both 5′ and 3′ ends of inserted vector sequence, reverse transcriptase (RT)-PCR confirmed the *msac1::β-GEO* insertion generates an mRNA where *mSac1* exon 1 is spliced to vector sequence (data not shown).

Creation and Genotyping of SAC1 Mice

Bay Genomics line NPX473 ES cells are annotated to have a pGT1dTM splice-trap insertion in intron 1 of the *SAC1* gene, which presents a splice-acceptor sequence upstream of a reporter gene *β-GEO*. The precise pGT1dTM insertion site was mapped by PCR and confirmed to reside in *SAC1* intron 1. $SAC1^{+/0}$ ES cells were injected into C57BL/6 blastocysts, and then they were implanted into pseudopregnant foster mothers. Male chimeric mice competent for germ line transmission of the *sac1::β-GEO* null allele were isolated and mated with wild-type C57BL/6 females to generate $SAC1^{+/0}$ mice. Genotypes of offspring derived from $SAC1^{+/0}$ mouse intercrosses were identified by a three primer PCR assay by using a shared forward primer (120bp@Intron1-F), a genomic reverse primer (630bp@Intron1-R), and an insertion-specific reverse primer (1kb@pGTM-R) to amplify wild-type *SAC1* and mutant *sac1* alleles (56°C annealing temperature; primer sequences Supplemental Table S1). When necessary, two amplification cycles were performed in nested PCR assays with the first cycle by using primers as described above. In the second cycle, primers 310bp@Intron1-F and 1kb@pGTM-R were used to amplify the mutant allele and primers 310bp@Intron1-F and 630bp@Intron1-R were used to amplify the wild-type allele. The PCR products are 330 and 240 bp for wild-type and mutant alleles, respectively. Staged embryos, blastocysts, and postimplantation embryos were collected according to published protocols (Nagy *et al*., 2003).

Cell Culture and Transfections

HeLa cells were cultured in DMEM supplemented with 10% fetal bovine serum, 100 μg/ml penicillin, and 100 μg/ml streptomycin. Transfections used Lipofectamine reagent (Invitrogen, Carlsbad, CA) according to manufacturer's instructions.

siRNA-mediated Gene Silencing

hSAC1 siRNA duplexes were from Dharmacon RNA Technologies (Lafayette, CO). HeLa cells were transfected with *hSAC1* siRNA, or control siRNA, with Lipofectamine reagent as described above. Total RNA was recovered from *SAC1* siRNA-treated and control cells 48 h after transfection and efficiency of silencing was monitored by reverse transcription (RT)-PCR. PCR primers were as follows: forward, 5′-ATGTTCCTCCTTCAGCTGTC-3′ and reverse, 5′-TCAGGACTAGTGTT GGATAGC-3′. Individual and combinatorial knockdown of ADP-ribosylation factor (*ARF*)*1* and *ARF4* expression was accomplished as described previously (Volpicelli-Daley *et al*., 2005).

Fluorescence Microscopy and Video Processing

Cells were plated onto coverslips and treated with *SAC1* siRNA oligonucleotides (oligos). Forty-eight to 72 h after siRNA treatment, control siRNA and *SAC1* siRNA-treated cells were fixed with 3.7% paraformaldehyde in phosphate-buffered saline (PBS) for 15 min, permeabilized with 0.2% Triton X-100 in PBS for 4 min, and washed with PBS. Permeabilized cells were blocked with 2% bovine serum albumin (BSA) in PBS for 1 h, and then they were incubated with respective antibodies in 2% BSA/PBS for 1 h. Cells were incubated with primary antibodies for 1 h, washed four times (5 min each wash) with PBS, and then incubated with fluorochrome-conjugated secondary antibodies for 1 h. Finally, cells were washed four times (5 min each wash) with PBS, and coverslips were mounted in Fluosave (Calbiochem, San Diego, CA). Cells were visualized by confocal microscopy (Leica SP2 aobs confocal [Wetzlar, Germany] or Zeiss 510 laser scanning confocal [Carl Zeiss, Jena, Germany]). All images were processed using Adobe Photoshop 6 (Adobe Systems, Mountain View, CA). Z-stack images of single cells were obtained (step size was 0.2–0.3 μm), and they were projected into videos by using LSM image browser software (Carl Zeiss).

Vesicular Stomatitis Virus Glycoprotein (VSV-G) Transport Assays

HeLa cells treated with control or *SAC1* siRNA were seeded onto coverslips and 24 h after transfection, cells were transfected in a second round with pEVFP-N1-VSV-G *tsO45* (FuGENE transfection; Roche Diagnostics, Mannheim, Germany). Four hours after transfection, cells were shifted to 40°C and incubated overnight at that temperature in growth medium. To study the ER–Golgi–plasma membrane transport, cells were shifted to 32°C for various times, fixed with 3.7% paraformaldehyde in PBS, and stained with anti-GM130 antibody. To block VSV-G export from the *trans*-Golgi network (TGN), cells were shifted from 40 to 32°C for 15 min, and then they were incubated at 20°C for 2 h. The TGN block was released by shift to 32°C for the indicated times, and cells were processed for immunofluorescence microscopy. The ratio of TGN VSV-G and total VSV-G fluorescence was then calculated. In all cases, 100 μg/ml cycloheximide was added 30 min before the temperature downshift.

Silence-Rescue System

A rescue sequence was generated though cloning the wild-type or mutant cDNA of *mSAC1* into the pLentiLox 4.0 pLL4.0 vector. Rescue sequence expression is under the control of the moderate UbC promoter, and the rescue open reading frame is fused to a C-terminal green fluorescent protein (GFP) tag to facilitate analysis. The wild-type *mSAC1* was amplified from mouse brain mRNA by reverse transcriptase-PCR by using primers MfeI site flanked forward primer, 5′-GGGCAATTGGCCACCATGGCGGCCGCAGCCT ACGAGCATC-3′; and BamHI site flanked reverse primer, 5′-CGGGATCCTCTCAGTCTATCTTTTCTTT CTGGAC-3′. The PCR products were digested by MfeI and BamHI and subcloned into the pLL4.0 vector though EcoRI and BamHI sites. The $msac1^{D391N}$ and $msac1^{R480H}$ mutants were generated by mutagenic primers as described above. The $msac1^{AEAID}$ mutant was generated by PCR by using the following mutagenic primers: 5′-CCCAGACTGGTCCAGGCAGAAGCGATAGACGGCGGAGGC-3′ and 5′-GC CTCCGCCGTCTATCGCTTCTGCCTGGACCAGTCTGGG-3′. Correct clones were isolated and virus was produced by transfecting human embryonic kidney (HEK)293 cells and collecting supernatant (Rubinson *et al*., 2003). Supernatant was then used to infect HeLa cells to generate stably transfected HeLa cell lines. The stable cell lines were selected by fluorescence-activated cell sorting (FACS) using GFP luminescence as positive signal.

FACS Analysis

Cells were trypsinized and then dispersed in PBS supplemented with 5% fetal bovine serum to obtain a single cell suspension. FACS was performed at the University of North Carolina-Chapel Hill School of Medicine FACS facility.

Glycosaminoglycan (GAG) Release Assays

GAG assays were performed on control- or *hSAC1* siRNA-challenged HeLa cells, as described previously (Litvak *et al*., 2005).

Cell Synchronization via Thymidine Block

Cell cultures were first incubated in medium containing 2 mM thymidine for 19 h. Cells were subsequently washed two times with PBS and fed with fresh media lacking thymidine. After a 9-h incubation, the medium was exchanged for fresh medium supplemented with 2 mM thymidine, and the cultures were incubated for an additional 16 h. Alternatively, to arrest cells in mitosis, cultures were incubated in medium containing 100 nM nocodazole for 12–14 h.

5-Bromo-2′-deoxyuridine (BrdU) Incorporation Assays

Cells grown on coverslips were labeled with 10 μM BrdU (Sigma-Aldrich, St. Louis, MO) for 2 h, and then they were fixed with 100% methanol for 10 min at −20°C. The slides were subsequently incubated in 2 N HCl for 1 h at 37°C to denature DNA, and washed twice for 10 min in 0.1 M borate buffer, pH 8.5, to neutralize the acid. After three washes with PBS, slides were incubated with Alexa Fluor 488-conjugated anti-BrdU antibodies (Invitrogen) diluted in PBS containing 0.1% BSA for 1 h, washed three times for 10 min each, mounted, and visualized by confocal microscopy. For FACS analysis, cells grown to 90% confluence in 60-mm dishes were incubated with 10 μM BrdU containing media for 2 h. Labeled cells were trypsinized, harvested by centrifugation, suspended in 0.5 ml of PBS, and fixed in 4.5 ml of 100% ethanol overnight at −20°C. Fixed cells were centrifuged at 1000 rpm for 5 min and then digested with 3 ml of 0.08% pepsin in 0.1 N HCl at 37°C for 20 min. Nuclei were pelleted, denatured with 1.5 ml of 2 N HCl at 37°C for 20 min, and neutralized with 3 ml of 0.1 M sodium borate. Nuclear pellets were washed with IFA buffer (10 mM HEPES, pH 7.4, 150 mM NaCl, 4% fetal bovine serum, 0.5% Tween 20, and 0.1% NaN_3) and incubated with 100 μl of Alexa Fluor 488-conjugated anti-BrdU antibodies diluted 1:5 in 0.5% IFA buffer at room temperature for 2 h. Nuclei were pelleted, washed with IFA buffer, resuspended in 500 μl of running buffer (0.5% IFA buffer, 200 μg/ml RNase A, and 1 μg/ml propidium iodide), and processed for FACS.

Online Supplemental Material

Supplemental Figure S1 shows the domain organization of Sac1 phosphatases. Supplemental Figure S2 describes inactivation of the murine *SAC1* gene by gene trap. Supplemental Figure S3 describes the morbidity associated with Sac1 depletion. Supplemental Figure S4 shows hSac1 depletion specifically

affects disorganization of Golgi membranes. Supplemental Figure S5 documents increased cell and nuclear area in hSac1-depleted cells. Supplemental Figure S6 shows hARF depletion results in disorganization of Golgi membranes without affecting mitotic spindle organization. Supplemental Movies S1 and S2 depict Z-stack projections of *cis*- and *trans*-Golgi membranes in a representative wild-type cell from the perspective of the *x*-axis and *z*-axis, respectively. Supplemental Movies S3 and S4 depict Z-stack projections of *cis*- and *trans*-Golgi membranes in a representative hSac1-depleted cell with moderately dispersed Golgi from the perspective of the *x*-axis and *z*-axis, respectively. Supplemental Movies S5 and S6 depict Z-stack projections of *cis*- and *trans*-Golgi membranes in a representative hSac1-depleted cell with severely dispersed Golgi from the perspective of the *x*-axis and *z*-axis, respectively. Supplemental Movie S7 shows the process of Golgi dispersal upon hSac1 depletion in living cells. Supplemental Movie S8 demonstrates hSac1-depleted cells with multipolar spindles present only two centrosomes.

RESULTS

Murine Sac1 Is a PIP Phosphatase

Ablation of ySac1 PIP phosphatase function evokes pleiotropic phenotypes that include a cold sensitivity for growth, Ins auxotrophy, allele-specific genetic interactions with mutations in the single yeast actin structural gene, and bypass for the normally essential cellular requirement for Sec14, the major yeast PtdIns/phosphatidylcholine transfer protein (Cleves *et al*., 1989; Novick *et al*., 1989; Whitters *et al*., 1993). Mutations that compromise ySac1 enzymatic activity phenocopy *sac1* null mutations, whereas substitutions outside the ySac1 catalytic motif evoke defects that are likely regulatory in nature (Nemoto *et al*., 2000; Li *et al*., 2002). Several lines of evidence demonstrate mSac1 shares a functional relationship to ySac1. mSac1 expression in *sac1*Δ yeast rescued the Ins auxotrophy of these strains (Figure 2A). Phenotypic rescue requires lipid phosphatase activity as evidenced by the inability of "catalytic-dead" mSac1^{D391N} missense mutant expression to restore growth to *sac1*Δ yeast under inositol-limiting conditions (Figure 2A). By contrast, other missense substitutions that correspond to ySac1 LOF mutations do not strongly compromise mSac1 activity. mSac1^{A442V} or mSac1^{R480H} (i.e., analogues of the yeast *sac1-10* and *sac1-22* gene products, respectively; Nemoto *et al*., 2000) expression rescued Ins-auxotrophy in the *sac1*Δ mutant (Figure 2A). These results were recapitulated for other *sac1*Δ-associated phenotypes, e.g., cold sensitivity for growth and "bypass Sec14" (data not shown).

PIP analyses from yeast radiolabeled with [^{3}H]Ins were consistent with the phenotypic rescue data. As demonstrated previously (Guo *et al*., 1999; Rivas *et al*., 1999; Hughes *et al*., 2000), ySac1 insufficiencies lead most strikingly to an increase in PtdIns-4-P mass with modest elevation in PtdIns-3-P. Whereas PtdIns-4-P and PtdIns-3-P constituted 0.8 ± 0.1 and 1.1 ± 0.1% of total Ins glycerophospholipid in wild-type yeast, these values rose to 10.4 ± 1.7 and 1.6 ± 0.3% in the *sac1*Δ mutant (Figure 2B). PtdIns-4,5-P_2 and PtdIns-3,5-P_2 species exhibited only subtle changes upon ySac1 LOF (data not shown). mSac1 expression in *sac1*Δ yeast restored PtdIns-4-P and PtdIns-3-P to wild-type levels (1.6 ± 0.3 and 0.9 ± 0.2%), whereas mSac1^{D391N} expression was ineffective (PtdIns-4-P and PtdIns-3-P values of 8.4 ± 0.4 and 1.7 ± 0.4% in the *sac1*Δ mutant, respectively; Figure 2B). mSac1^{A442V} or mSac1^{R480H} expression also corrected *sac1*Δ-associated derangements in PIP homeostasis. The mSac1^{A442V}-expressing *sac1*Δ yeast strain exhibited fractional values for PtdIns-4-P and PtdIns-3-P of 3.1 ± 0.8 and 1.3 ± 0.2%, respectively, whereas those values for the mSac1^{R480H}-expressing *sac1*Δ mutant were 2.8 ± 0.8 and 1.5 ± 0.1% (Figure 2B).

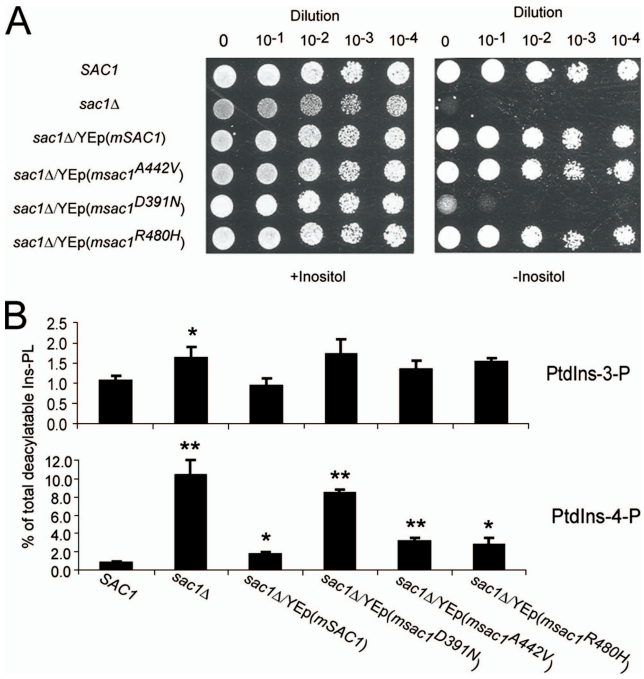

Figure 2. mSac1 is a PIP phosphatase. (A) mSac1 complements ySac1 defects. Strain CTY244 (*sac1*Δ) was transformed with yeast episomal plasmids that drive expression of *mSAC1*, mutant *msac1* alleles encoding mSac1^{D391N}, mSac1^{A442V}, and mSac1^{R480H}, respectively, as well as a *URA3* control. Strains were spotted in 10-fold dilution series onto Ins-replete and Ins-depleted media and incubated at 26°C for 4 d. (B) PIPs in *sac1*Δ strains. *SAC1* yeast, and isogenic *sac1*Δ mutants carrying YEp(*URA3*), YEp(*mSAC1*), YEp(*msac1^{D391N}*), YEp(*msac1^{A442V}*), or YEp(*msac1^{R480H}*) were labeled with [^{3}H]Ins for at least 18 h, PLs were extracted and deacylated in the presence of methylamine, and the glycerol-phosphoinositol species were resolved by anion exchange chromatography and quantified. PtdsIns-3-P and PtdIns-4-P are represented as percentages of total deacylatable Ins-phospholipid (PL). Data are expressed as mean values calculated from at least three independent experiments. Standard deviations are given (*$p < 0.01$ and **$p < 0.001$).

Sac1 and Cargo

A stable HeLa cell line was generated that expresses a functional mSac1-GFP chimera. The expression level for the ectopically expressed mSac1-GFP was approximately threefold greater than that of endogenous hSac1 (see below). Under those conditions, mSac1-GFP colocalized with an ER marker (calnexin), a *cis*-Golgi marker (GM130), and a TGN marker (TGN46; Figure 3A). This pattern is in agreement with the distribution of endogenous Sac1 in mammalian cells (Nemoto *et al*., 2000; Rohde *et al*., 2003). mSac1-GFP showed a higher degree of colocalization with the *cis*-Golgi marker GM130 than with the TGN marker TGN46 (Figure 3A). The presence of mSac1 in Golgi cisternae (particularly TGN) is paradoxical given PtdIns-4-P is important for anterograde trafficking from the TGN (Hama *et al*., 1999; Walch-Solimena and Novick, 1999; Godi *et al*., 2004). One possibility is mSac1 is disqualified from efficient entry into Golgi subregions from which anterograde vesicles bud.

To investigate whether mSac1 is indeed excluded from such subregions of mammalian Golgi membranes, the colocalization of mSac1-GFP with an anterograde cargo molecule was monitored. The cargo marker was represented by a red fluorescent protein (RFP)-tagged version of the *tsO45* mutant version of VSV-G protein (RFP-*tsO45*-VSV-G). The mSac1-GFP–expressing HeLa cell line was transfected with

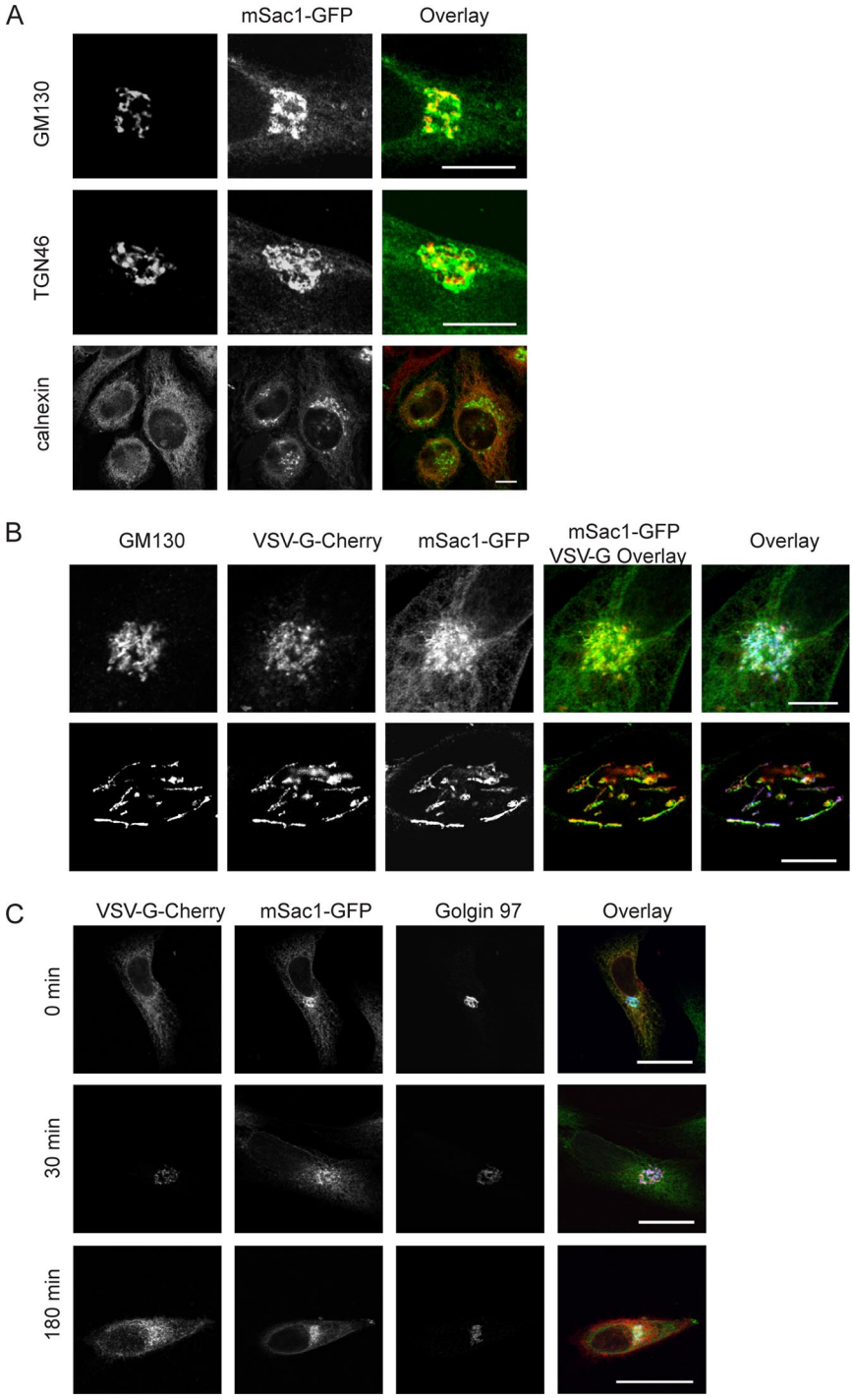

Figure 3. Localization of ectopically expressed mSac1 in HeLa cells. (A) A stable cell line expressing mSac1-GFP was stained with antibodies directed against GM130, TGN46, or α-calnexin. Bars, 10 μm. (B) HeLa cells stably expressing mSac1-GFP were transiently transfected with plasmids that drive expression of RFP-*tsO45*-VSV-G. *cis*-Golgi membranes were marked by GM130. Merged images highlight colocalization of mSac1-GFP with RFP-*tsO45*-VSV-G cargo. Bars, 10 μm. (C) mSac1-GFP HeLa cells were transfected with the plasmid expressing RFP-*tsO45*-VSV-G. Four hours after transfection, cells were shifted to 40°C and incubated overnight to trap the newly synthesized RFP-*tsO45*-VSV-G in the ER. The retained ER pool was released into the secretory pathway by downshift to 32°C for the indicated time periods. Cells were fixed, immunostained for Golgin-97, and processed for immunofluorescence microscopy. Bars, 20 μm.

constructs driving RFP-*tsO45*-VSV-G expression. Transfected cells were incubated at 40°C to accumulate biosynthetic RFP-*tsO45*-VSV-G in the ER (Presley *et al*., 1997; Scales *et al*., 1997). A wave of RFP-*tsO45*-VSV-G was then released from the ER into the secretory pathway by downshift of cells to 32°C. Partial colocalization of mSac1-GFP with RFP-*tsO45*-VSV-G was recorded when this cargo was transported from ER to the Golgi (Figure 3B). However, mSac1-GFP did not follow the RFP-*tsO45*-VSV-G cargo wave from Golgi to the plasma membrane (Figure 3C). The data indicate mSac1 partially incorporates into cargo-containing subregions of Golgi membranes. This incorporation is most pronounced in *cis*-Golgi compartments, but it is not obvious in late Golgi compartments.

Murine Sac1 Nullizygosity Results in Early Embryonic Lethality

Reproductive activity of $msac1^{0}$ sperm and eggs is not affected. Cross of $mSAC1^{+/0}$ males to $mSAC1^{+/+}$ females, and, reciprocally, $mSAC1^{+/0}$ females to $mSAC1^{+/+}$ males yielded heterozygous progeny at frequencies approximating the expected 50% value (52 $mSAC1^{+/+}$: 61 $mSAC1^{+/0}$ and 24 $mSAC1^{+/+}$: 31 $mSAC1^{+/0}$, respectively). However, genotypic analysis of live progeny derived from intercross of

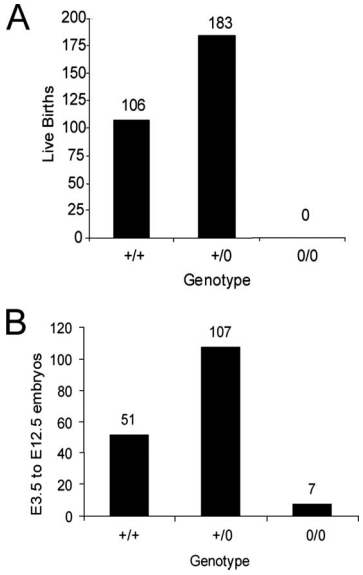

Figure 4. Preimplantation lethality of *msac1*$^{0/0}$ mice. (A and B) Genotypic distributions. *mSAC1* genotypes of the 289 live-born F1 progeny produced by intercrosses of *SAC1*$^{+/0}$ mice (A), as well as the 165 F1 embryos harvested in an E3.5–E12.5 window from parallel heterozygote matings (B) are shown.

SAC1$^{+/0}$ animals indicate *msac1::β-GEO* is a lethal and fully penetrant autosomal recessive mutation (Figure 4A). Further analyses revealed early developmental failure for mSac1-deficient animals. Of the 178 embryos harvested in the developmental window ranging from E3.5 to E12.5 (96 of which were collected at E3.5), a genotypic distribution of 51 *mSAC1*$^{+/+}$; 107 *mSAC1*$^{+/0}$; 7 *msac1*$^{0/0}$ was recorded (Figure 4B). Of the seven *msac1*$^{0/0}$ progeny recovered, a single grossly malformed embryo was recovered at embryonic day (E)7.5. The remaining embryos were recovered at the E3.5 blastocyst stage with no obvious structural abnormalities. In sum, we recovered a genotypic distribution of 157 *mSAC1*$^{+/+}$; 290 *mSAC1*$^{+/0}$; 7 *msac1*$^{0/0}$. In total, 13 resorptions occurred during the E7.5–E11.5 developmental window. The preimplantation lethality suggests mSac1 executes an essential housekeeping function. In support of this conclusion, challenge of HeLa cells with siRNA directed against human *SAC1* (*hSAC1*) mRNA results in clear and specific compromise of cell viability (Supplemental Figure S3A). Flow cytometry analyses recorded significant elevations in the sub-G1 (morbid or dead cell) load in hSac1-depleted cell populations (Supplemental Figure S3B). Consistent with a nonapoptotic pathway for cell death, morbidity of hSac1-deficient cells was not rescued by pharmacological challenge with the pan-caspase inhibitor Z-VAD-fmk (data not shown).

hSac1 Deficiencies Evoke Structural Derangements of the Golgi System

The morbidity of Sac1-deficient mammalian cells, when coupled with the ER/Golgi localization of this PIP phosphatase, implicated ER and/or Golgi membranes as likely casualties of Sac1 dysfunction. To assess the functional competence of the ER and Golgi systems under conditions of Sac1 insufficiency mammalian cells, the siRNA approach was again used with HeLa cells as primary experimental model. Given *mSAC1*$^{+/0}$ mice exhibit no overt phenotype, and given that embryonic fibroblasts derived from *mSAC1*$^{+/0}$ mice are robust, the cellular Sac1 threshold for functional sufficiency is necessary below 50% of wild-type expression levels. In that regard, the siRNA strategies used achieved bulk knockdown efficiencies of ~50–60% in HeLa cell populations as judged by RT-PCR (Figure 5A). Immunoblotting experiments confirmed that bulk hSac1 levels were reduced in siRNA-treated HeLa cell populations (Figure 5B). Because these data represent averaging estimates, we think it most likely silencing efficiency reflects a condition where a fraction of cells is effectively silenced for *hSAC1* expression, rather than a situation where all cells exhibit uniform reductions in *hSAC1* expression.

A dramatic phenotype associated with hSac1 depletion is disorganization of the Golgi system. Some 60% of HeLa cells in the hSac1-depleted condition exhibited dispersal of *cis*-, *medial*-, and *trans*-Golgi compartments to what we classify as "moderately dispersed" and "severely dispersed" arrangements. The moderately dispersed arrangement is defined by relaxation of the compact Golgi structure into a reticular arrangement, whereas the severely dispersed condition is typified by extensive fragmentation of the Golgi system (Figure 5C; see Supplemental Movies S1–S6). The Golgi dispersal phenotype, regardless of severity, was consistent throughout the stack, i.e., Golgi with severely dispersed *cis*-Golgi compartments exhibited severely dispersed TGN, whereas Golgi with moderately dispersed *cis*-Golgi presented moderate TGN dispersion. Incorporation of the pan-caspase inhibitor Z-VAD-fmk during the silencing protocol had no significant effect on the frequency of cells presenting deranged Golgi morphology upon hSac1 depletion (data not shown). These findings indicate onset of the Golgi morphology phenotype is not a consequence of activating apoptotic pathways. Time-lapse video microscopy of HeLa cells stably coexpressing a β-1,4-galactosyltransferase-GFP Golgi marker, and an mCherry-histone H2B nuclear marker, were challenged with *hSAC1* siRNA and imaged at 30 h post-siRNA treatment. Onset of Golgi disorganization is documented in Supplemental Movie S7. Of the 194 cells scored, 76% developed deranged Golgi organization—a frequency in accord with experiments where fixed cells were imaged.

The effects on Golgi structure represented specific effects of *hSAC1* silencing based on several criteria. First, the *hSAC1* siRNA-mediated Golgi dysmorphology was not limited to HeLa cells. The effect was recapitulated in other human cell lines such as HEK293 (Figure 5D). Moreover, neither the striking disruption of Golgi architecture, nor the reduction in Sac1 expression levels, was observed when nonhuman cells (e.g., COS-7) were treated with *hSAC1* siRNA oligonucleotides, or when HeLa cells were challenged with irrelevant *hPITPα* siRNA oligonucleotides (although *hPITPα* expression was effectively silenced; data not shown). Endomembrane specificity to the *hSAC1* siRNA effect was also observed. hSac1 depletion levied no obvious effects on lysosomal, endosomal, mitochondrial, or ER architecture (Supplemental Figure S4A). Finally, Golgi disorganization was rescued by expression of a silencing-resistant mSac1-GFP (see below).

Disorganized Golgi Retain Transport Competence

Three lines of evidence indicate structural compromise of Golgi membranes upon hSac1 depletion does not levy strong defects in anterograde membrane transport. First, the transport efficiency was monitored for a synchronized wave of *tsO45*-VSV-G trafficking from the ER to the Golgi system, and from the Golgi to the plasma membrane. No significant deviation was recorded between hSac1-depleted versus wild-type control cells in either transport stage (Figure 6, A–C). Second, [^{35}S]sulfate pulse-chase experiments demon-

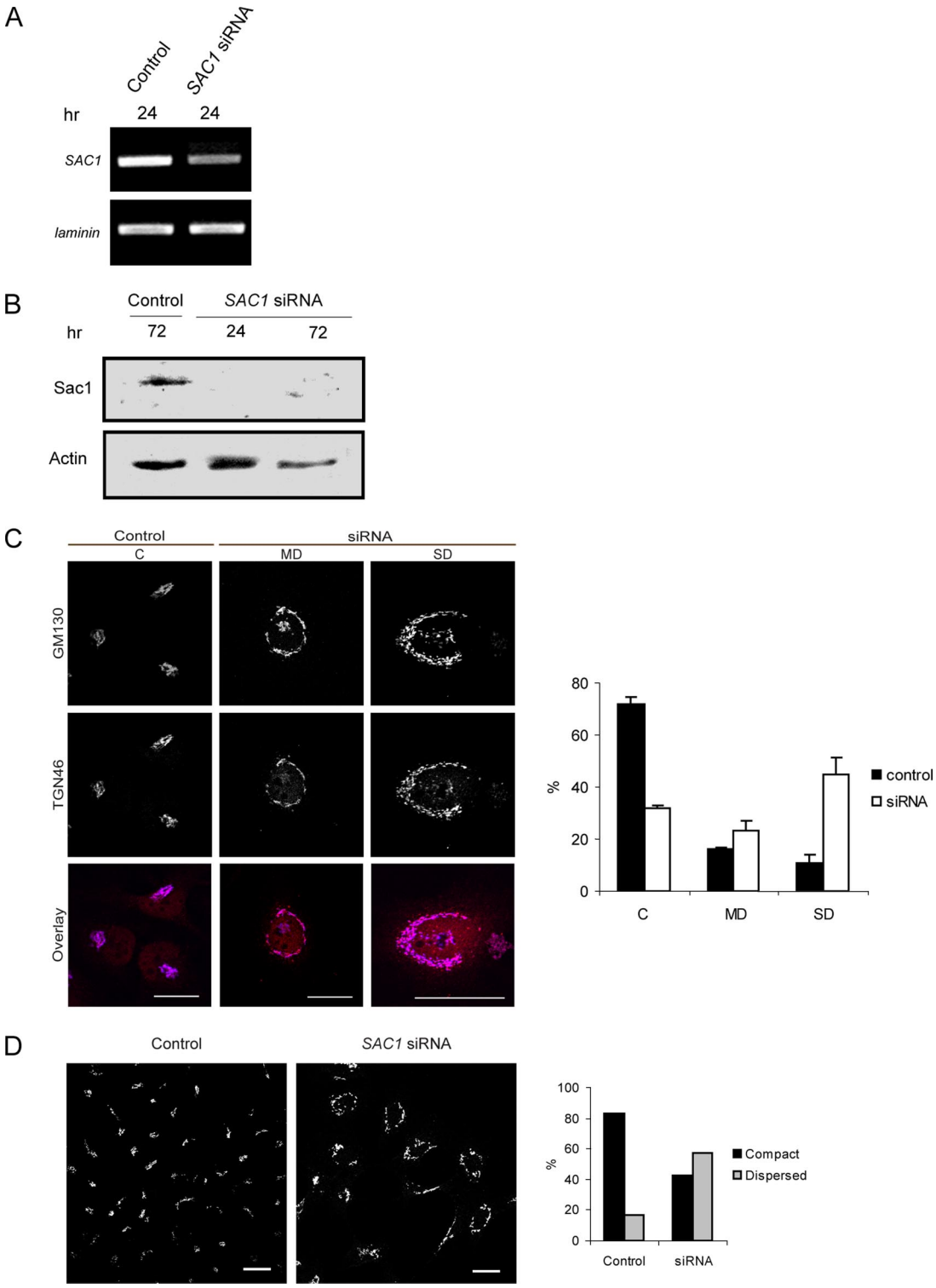

Figure 5. *hSAC1* silencing and Golgi morphology. (A) HeLa cells were challenged with *hSAC1* or control siRNA oligonucleotides, and total cell RNA was harvested after 24 h. The total RNA fraction was used to template cDNA synthesis by reverse transcription (RT), and the RT products were used to template amplification of a 300-base pair fragment of *hSAC1*. Reactions were normalized by amplification of a 300-bp product derived from laminin mRNA. (B) HeLa cells were treated with *hSAC1* or control siRNA oligonucleotides. After 24 and 72 h, hSac1 levels were analyzed by immunoblot from lysates prepared from 10^4 cells. Actin was monitored as normalizing control. (C) Forty-eight hours after *SAC1* siRNA treatment, HeLa cells were fixed and imaged for GM130 and TGN46. Representative images of *hSAC1* siRNA-treated, or control siRNA cells are shown. Golgi morphology was defined as "compact" (C), moderately dispersed (MD) or severely dispersed (SD). Distributions (expressed as percentages) of each category of Golgi membranes was compared for hSac1-depleted cells relative to controls (right). These were calculated as mean values (with standard deviations) from three independent experiments with >100 cells scored per experiment. Bar, 20 μm. (D) Golgi morphology in hSac1-depleted HEK293 cells. Over 60% of *hSAC1* siRNA cells exhibited dispersed Golgi membranes. Data were obtained from two independent experiments with >100 cells scored per experiment. Bar, 20 μm.

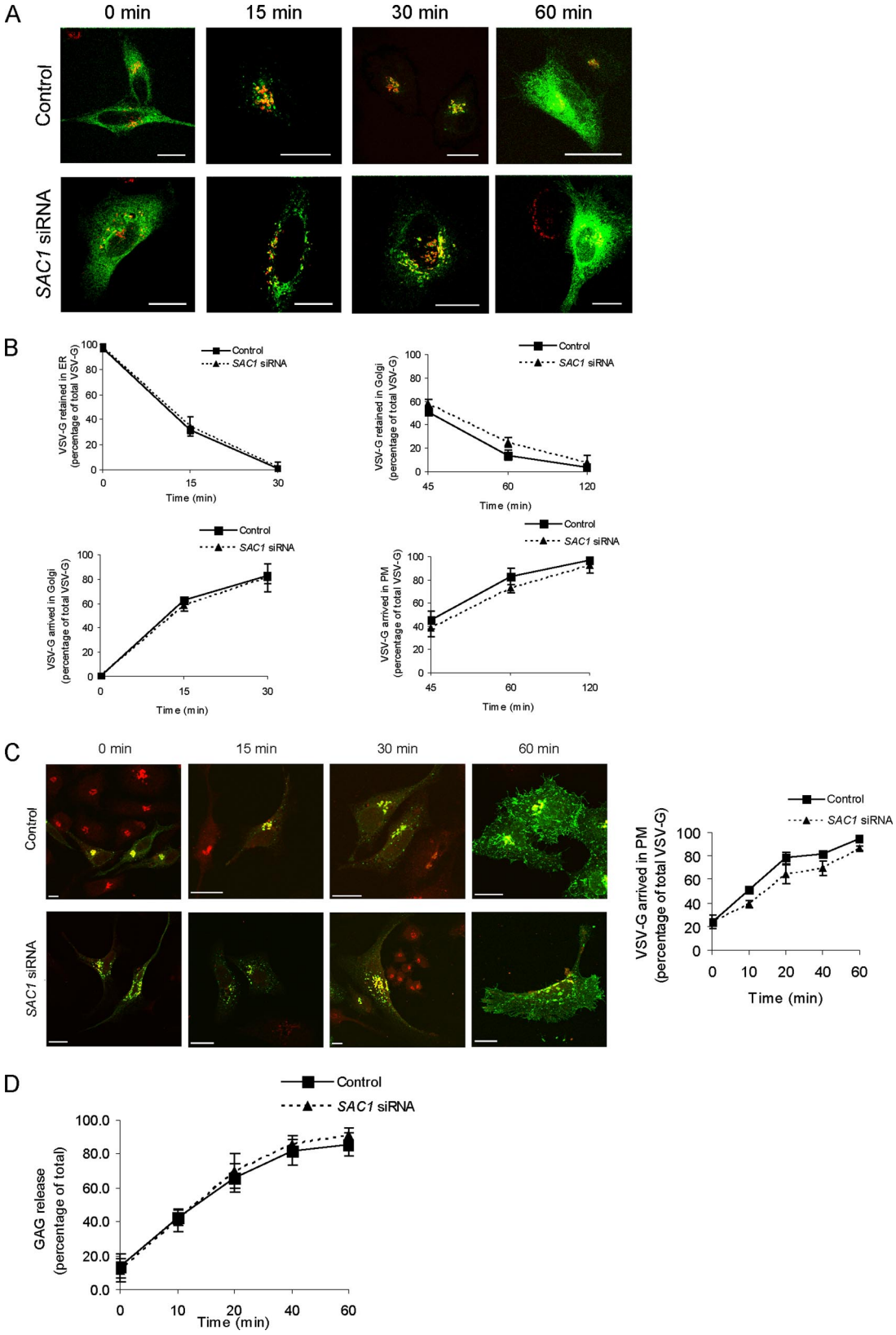

Figure 6. Sac1 depletion does not compromise membrane trafficking. (A and B) hSac1 depletion does not affect protein transport from the ER to the Golgi or from the Golgi to the plasma membrane. HeLa cells challenged with control and *hSAC1* siRNAs were transfected with a construct that expresses the temperature-sensitive mutant ts045-VSV-G-yellow fluorescent protein (YFP), incubated at 37°C for 4 h, and then at 40°C overnight to accumulate VSV-G in the ER. Cyclohexamide (100 μg/ml) was added to cells, and 30 min later cells were shifted to 32°C to release the VSV-G transport along the secretory pathway. Cells were fixed and imaged at different time points as indicated. The Golgi is visualized by staining with the GM130 antibody (red), and VSV-G-YFP is shown as green in the figure. The rate of VSV-G export from the

strated both rate and efficiency of transport of newly synthesized GAGs from the TGN to the plasma membrane were uncompromised in hSac1-depleted cells (Figure 6D). Third, [^{35}S]methionine pulse-chase analyses in hSac1-depleted cell cultures, reported normal biosynthetic transport of transferrin receptor from ER to Golgi, as assayed by conversion of core-glycosylated transferrin receptor to an endoglycosidase H-resistant state (data not shown).

The possibility that hSac1 deficiency evokes mislocalization of PtdIns-4-P-binding proteins from the Golgi complex was considered. Such an effect could arrive as a consequence of PtdIns-4-P accumulating to high levels on inappropriate membrane surfaces, e.g., ER (Li *et al*., 2002). [^{3}H]Inositol radiolabeling experiments, coupled with analyses of PIP species, reports a modest but reproducible (~30%) increase in PtdIns-4-P in hSac1-deficient cell populations relative to controls (Supplemental Figure S4B). Given the silencing efficiency, this translates to an ~50–60% increase in cellular PtdIns-4-P in depleted cells. To determine whether such increase is of sufficient magnitude to redistribute PIP binding proteins, we followed the localization of endogenous TGN-associated PIP-binding proteins under conditions of Sac1 depletion. These include the two FAPP proteins (FAPP1 and FAPP2) whose localization to TGN membranes is controlled by a pleckstrin homology (PH)-domain that binds PtdIns-4-P (Godi *et al*., 2004). The targeting fidelity of an FAPP1 PH-domain-mCherry reporter was maintained in hSac1-depleted HeLa cells with dispersed Golgi membranes (Figure 7A). Association of endogenous FAPP1 and FAPP2 with HeLa TGN was similarly undisturbed (data not shown). Localization of Orp9, a Golgi-targeted member of the oxysterol binding protein family (Lessmann *et al*., 2007; Wyles and Ridgway, 2004), was also unimpressed by hSac1 depletion (Figure 7B). The structurally deranged Golgi system in hSac1-depleted cells retained its cohort of other peripheral Golgi proteins as well, including β-COP (Chen *et al*., 2005; Duden *et al*., 1991; Oprins *et al*., 1993) (Figure 7C) and the TGN-associated phosphatidylinositol transfer protein (PITP)β (Phillips *et al*., 2006) (Supplemental Figure S4C). Finally, as the severely dispersed Golgi phenotype of hSac1-depleted cells is similar to the effects imposed by nocodazole challenge, we also monitored status of microtubules (MTs) in such cells. The MT cytoskeleton was superficially normal in hSac1-deficient cells, even in those with highly fragmented Golgi membranes (Figure 7D).

Figure 6 (cont). ER to the Golgi, and from the Golgi to the plasma membrane was measured by comparing the ratio of ER-associated, Golgi-associated VSV-G, and plasma membrane-associated VSV-G to total VSV-G fluorescence for each time point. Data are from three independent experiments, with >100 cells imaged per time point per experiment. Bar, 20 μm. (C) *hSAC1* silencing does not affect protein transport from the Golgi to the plasma membrane. The Golgi is visualized by a TGN marker, TGN46 antibody (red), and VSV-G-YFP is rendered green in the figure. Rate of VSV-G export from the Golgi to the plasma membrane was estimated by comparing the ratio of Golgi-associated VSV-G, and plasma membrane-associated VSV-G to the total VSV-G fluorescence for each time point. The data are from three independent experiments, with >100 cells per time point per experiment. Bar, 20 μm. (D) hSac1 depletion does not inhibit release of [^{35}S]GAGs from HeLa cells. Control and *hSAC1*-depleted HeLa cells were incubated with xyloside (15 min), pulse-labeled with [^{35}S]sulfate (5 min), and then chased for the indicated times. [^{35}S]GAGs were precipitated from supernatant and cell pellet fractions with cetylpyridinium chloride, and quantified. The radioactivity of [^{35}S]GAGs in the supernatant was compared with total radioactivity, presented as a percentage, and plotted against time. Data are from three independent experiments.

hSac1 Depletion and Cell Spreading

Another prominent morphological feature of cells treated with *hSAC1* siRNAs is an approximately 2.3-fold increase in cell spreading area (2325 $\pm$ 791 μm^2) relative to controls (995 $\pm$ 228 μm^2; Supplemental Figure S5A). Increased cell spreading correlated with magnitude of Golgi structural derangement. That is, HeLa cells with severely dispersed Golgi membranes exhibited pronounced increases in cell spreading area (2958 $\pm$ 1246 μm^2; 2.9-fold increase relative to mock control cells), and those with moderately dispersed Golgi showed moderate increases in cell spreading area (1754 $\pm$ 530 μm^2; approximately an average 1.8-fold increase relative to mock control cells). hSac1-depleted HeLa cells also exhibited larger nuclei compared with controls, and the magnitude of nuclear enlargement was directly proportional to cell spreading area and severity of the Golgi architectural derangement. Those cells with moderately and severely dispersed Golgi membranes exhibited ~1.3- and 2.0-fold enlargements in nuclear area compared with controls, respectively (Supplemental Figure S5B).

The large increases in cell spreading area suggested cytoskeletal alterations in hSac1-depleted cells. One mechanism for inducing such increases in cell surface area is diminished formation of dorsal filopodia (Bohil *et al*., 2006). However, scanning electron microscopy revealed no significant reductions in dorsal surface filopodial density in hSac1-insufficient cells (0.34 $\pm$ 0.14 filopodia/μm^2) compared with controls (0.46 $\pm$ 0.09 filopodia/μm^2). Functional ablation of ySac1 alters yeast actin organization (Novick *et al*., 1989), an effect interpreted as an indirect consequence derived from deregulated interactions between actin binding proteins and PIPs (Cleves *et al*., 1991; Whitters *et al*., 1993). Visualization of F-actin by phalloidin staining showed no dramatic disorganization of actin stress fibers in hSac1-depleted cells, although stress fibers seemed more pronounced relative to those in controls (Supplemental Figure S5C).

hSac1 and Organization of the Mitotic Spindle

To investigate cell cycle progression in hSac1-depleted cells more directly, an asynchronous HeLa cell population was challenged either with control or *SAC1* siRNAs, and BrdU incorporation and propidium iodide staining were both monitored as readouts for DNA content. Relative to controls, hSac1-depleted populations exhibited fewer cells in S phase 48 h after siRNA challenge (26 vs. 14%, respectively). This decrease was accompanied by a compensating increase in the G2/M population (4 vs. 15% of total cells, respectively; Figure 8A). Experiments where cells were synchronized at the G1/S boundary by a double-thymidine block strategy (see *Materials and Methods*) further buttressed these findings. At 12 h after release from G1/S arrest, cells with severely or moderately dispersed Golgi membranes were underepresented in the S phase cell population relative to controls (32 vs. 46 vs. 74%, respectively; Figure 8B), suggesting that cells with disorganized Golgi membranes do not progress efficiently though G2/M. To assess the effects of hSac1 depletion on cell cycle progression though G2/M phase, *hSAC1* siRNA treated and control cells were arrested in mitosis by nocodazole treatment (100 nM) for 12–14 h. Arrested cells were fixed, permeablized, and double-labeled for α-tubulin and DNA. Consistent with a difficulty for hSac1-depleted cells to traverse G2/M, only ca. 1% of the cells in hSac1-depleted populations escaped from the nocodazole-induced prometaphase block and progressed to anaphase or telophase. This frequency is reduced relative to

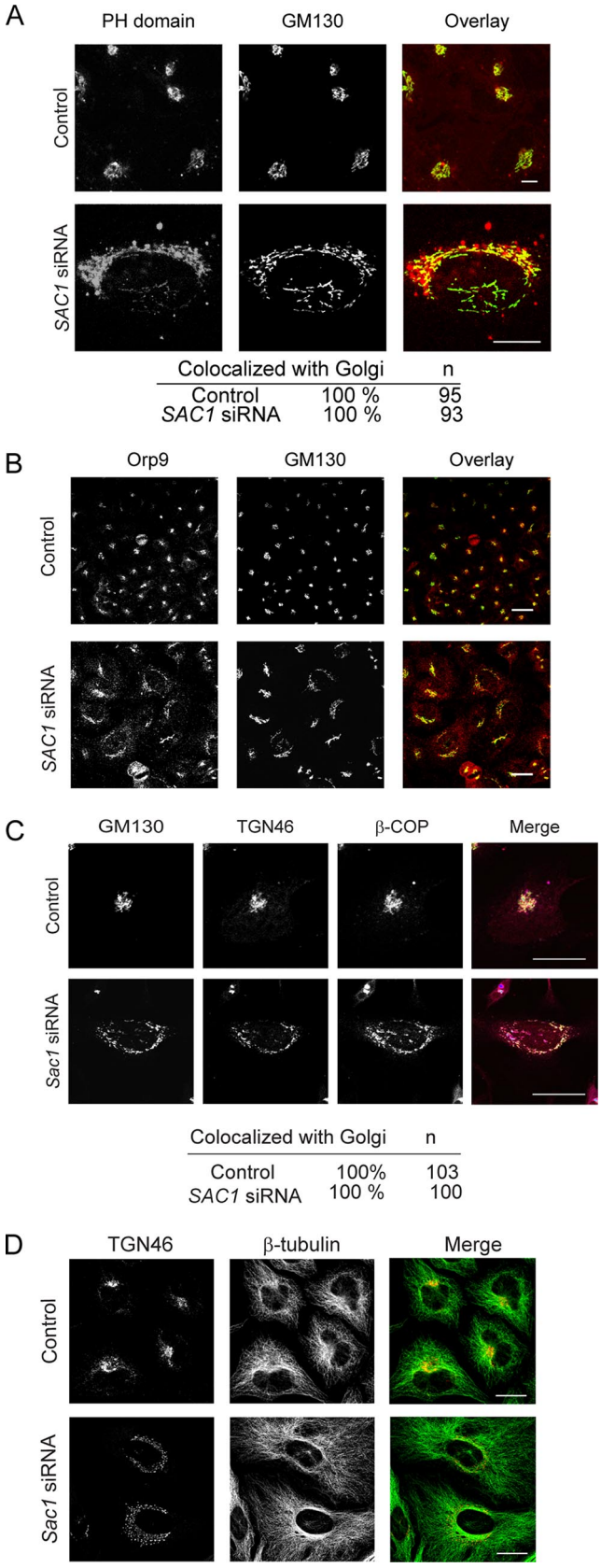

Figure 7. hSac1-deficiency and PIP-binding proteins. (A) Twenty-four hours post-siRNA treatment, control and *hSAC1* siRNA-challenged cells were transfected with a construct that expresses a FAPP1 PH-domain-cherry sensor for PtdIns-4-P. Twenty-four hours after transfection, cells were processed for immunofluorescence microscopy. Golgi membranes were visualized with GM130. Images are representative of those obtained in two independent experiments where >100 cells were scored per experiment. Bar, 10 μm. (B) hSac1-depleted HeLa cells were fixed, permeabilized, and codecorated with primary antibodies directed against endogenous Orp9 and GM130. Bar, 20 μm. (C and D) hSac1-depleted HeLa cells were fixed and decorated with antibodies directed against β-COP or β-tubulin. β-COP-stained cells were triple-stained with antibodies directed against the *cis*-Golgi marker GM130, and the *trans*-Golgi marker TGN46. Images shown are representative of >100 cells scored. Bar, 20 μm.

the >12% of control cells that escaped the G2/M arrest (Figure 8C).

In addition to the reduced frequency of hSac1-deficient escapers from the G2/M-arrested cell population, we observed an ~10-fold elevation in the frequency of mitotic hSac1-depleted cells with abnormal multipolar spindles (Figure 8C). These ectopic spindles were mechanically competent, because 4,6-diamidino-2-phenylindole (DAPI) staining indicated these spindles powered aberrant segregation of chromosomal material. Again, the increased incidence of cells with multipolar spindles in hSac1-depleted cell populations was not affected by treatment with the caspase inhibitor Z-VAD-fmk (data not shown). Multipolar spindles can result from deregulated centrosome duplication followed by MT nucleation at ectopic centrosomes (Hinchcliffe and Sluder, 2001; Khodjakov and Rieder, 1999). Thus, we surveyed the status of γ-tubulin (marks the ring structure that nucleates spindle MT assembly; Moudjou *et al*., 1996) and centrin-2 (a component of the centriole that regulates centriolar duplication; Salisbury *et al*., 2002). The data consistently reported multiple γ-tubulin foci in cells with multipolar spindles. Of the cells with multiple spindle asters; however, >95% presented only two centrin-2 foci. These data indicate centrosome duplication occurred normally in hSac1-deficient cells (Figure 9, A and B and Supplemental Movie S8).

Functional Properties of Mammalian Sac1

The Golgi morphological derangements and spindle disorganization associated with hSac1 depletion presented facile readouts for dissecting functional properties of mammalian Sac1. To that end, and to confirm that the Golgi and spindle structural defects reported a specific effect of reduced hSac1 function, wild type and mutant variants of a silencing-resistant *mSAC1-GFP* gene fusion were individually expressed in HeLa cells from a lentiviral expression vector. *mSAC1-GFP*–expressing cells were challenged with *hSAC1* siRNA oligonucleotides. Morphological status of the Golgi was assessed by monitoring distribution of the *trans*-Golgi marker TGN46, whereas spindle organization was monitored by visualization of α-tubulin. These parameters were followed in hSac1-depleted cells individually expressing 1) the mSac1-GFP chimera, 2) mSac1-GFP variants with graded compromise of Sac1 PIP phosphatase activity, or 3) mSac1-GFP derivatives incompetent for binding to the COP1 coatomer that regulates trafficking of this enzyme.

mSac1-GFP expression efficiently rescued the Golgi and spindle disorganization evoked by *hSAC1* siRNA challenge (Figure 10, A, B, and D). Similarly, expression of the substantially functional mSac1^{R480H}-GFP levied a partial, but significant, rescue of the same. mSac1-GFP expression also corrected the enhanced cell spreading of hSac1-depleted cells (data not shown). By contrast, expression of the catalytically inactive

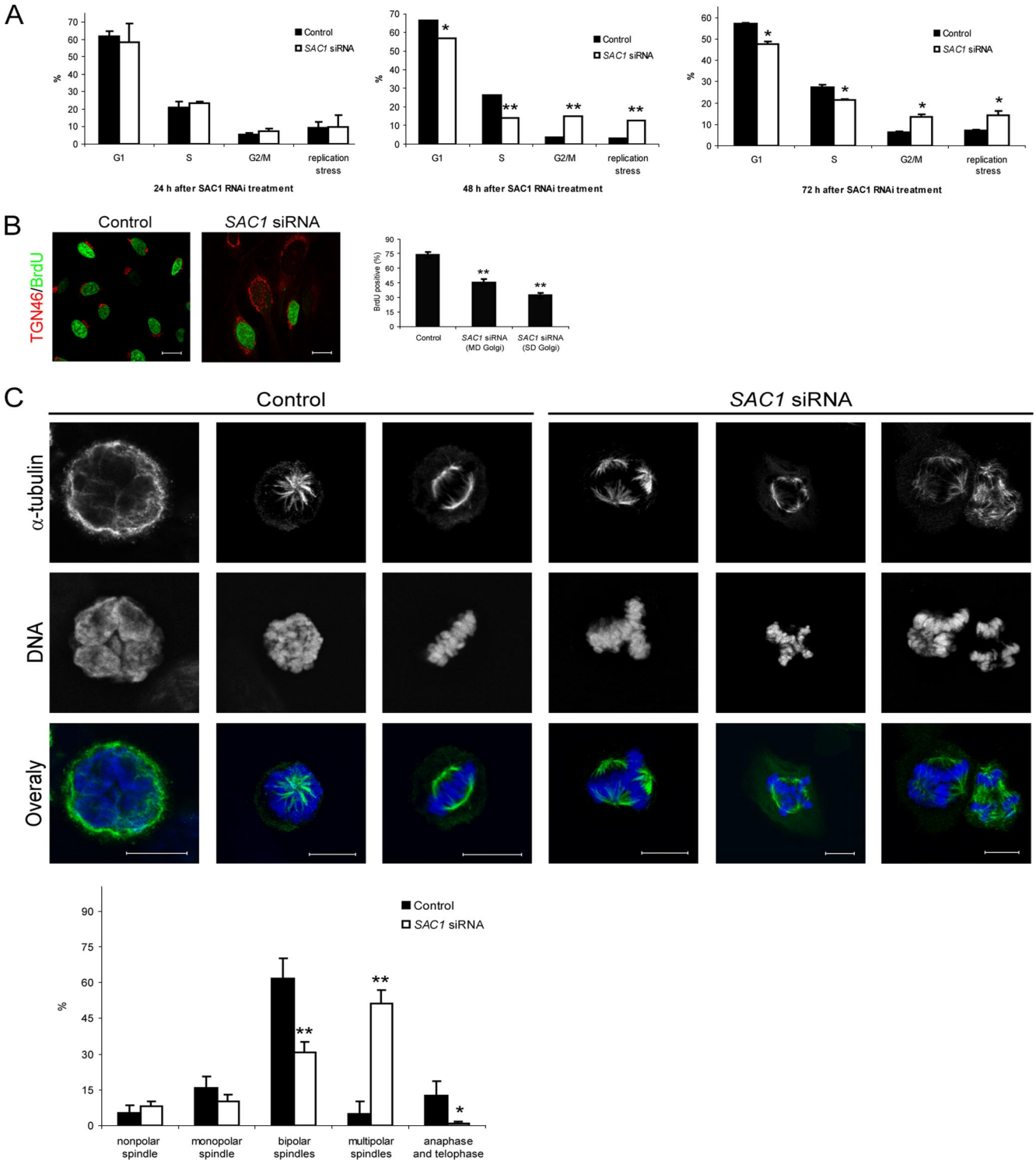

Figure 8. hSac1-depletion evokes mitotic defects. (A) At various times after transfection, *hSAC1*- or control siRNA-treated HeLa cells were incubated with BrdU-supplemented growth media for 3 h, trypsinized, fixed, stained with propidium iodide, and processed for FACS analysis. Some 10^4 cells were analyzed in each FACS experiment. Distribution of cells at different stages of the cell cycle (G1, S, G2/M, and replication stress) is shown as percentages of total cell number. The data either represent mean values from two independent experiments, or mean values with standard deviations from three independent experiments (*$p < 0.05$ and **$p < 0.001$). (B) *SAC1* and control siRNA transfected cells were synchronized at G1/S by double thymidine block and pulsed with BrdU for 2 h at 56 h after siRNA treatment. Cells were fixed and double stained with antibodies to BrdU (green) and the *trans*-Golgi marker TGN46 (red). Data are from two independent experiments, and >400 cells were examined from three independent transfections per experiment (**$p < 0.001$). Bar, 20 μm. (C) Thirty hours after siRNA challenge, *hSAC1* and control siRNA-challenged cells were incubated with growth media containing 100 nM nocodazole for 12–16 h to accumulate mitotic cells. Cells were fixed and stained for α-tubulin (green) and DAPI. Representative images of spindle and chromosome organization in control and Sac1 depletion conditions are shown. Data are from three independent experiments with three independent transfections per experiment. In total, >400 cells were examined (*$p < 0.01$ and **$p < 0.001$). Bar, 10 μm.

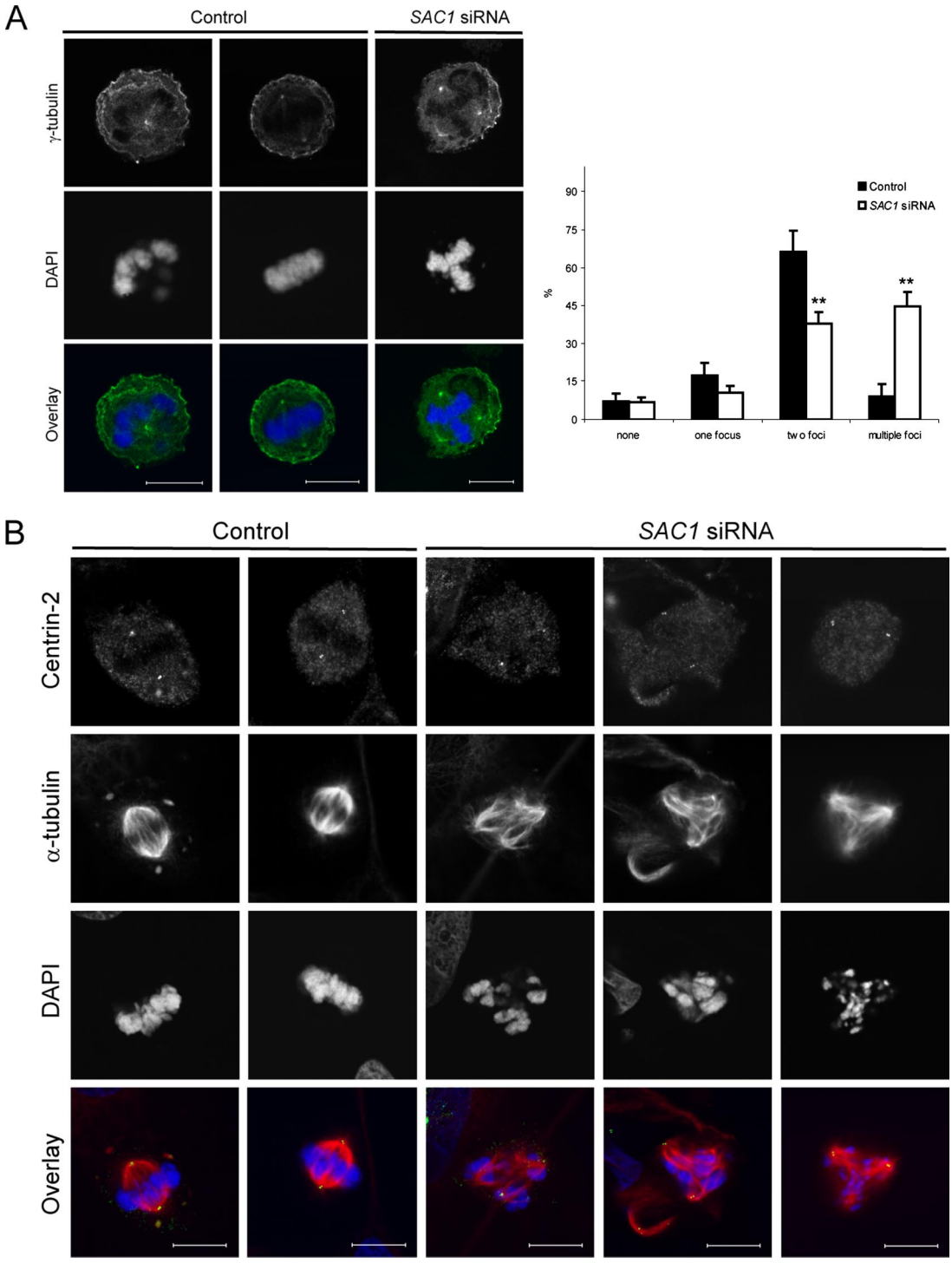

Figure 9. Centrosome duplication in hSac1-deficient cells. (A) Asynchronous cell populations challenged with *hSAC1*- or control siRNAs were stained for γ-tubulin (green) and DAPI. Representative images of γ-tubulin foci (centrosomes) and DNA are shown. Data were derived from three independent experiments, and >400 cells were examined from three independent transfections per experiment (**$p < 0.001$). Bar, 10 μm. (B) Experimental conditions were as described in A, except cells were stained for the centrosome marker centrin-2 (green), α-tubulin (red), and DAPI (blue). Representative images are shown. Only two centrin-2 foci are apparent in cells with multiple spindle asters. Bar, 10 μm.

mSac1^{D391N}-GFP was ineffective in correcting the structural derangements of either the HeLa Golgi system, or the spindle apparatus, in cells challenged with *hSAC1* siRNA oligonucleotides (Figure 10, A, B, and D). Mammalian Sac1 harbors a C-terminal $_{583}$KEKID$_{587}$ COP1-binding motif that promotes retrograde trafficking of this enzyme from Golgi compartments back to the ER. Inactivation of this motif by converting the K residues to A results in Sac1 accumulation in the Golgi system (Rohde *et al.*, 2003). Expression of mSac1^{AEAID}-GFP, a mutant mSac1 for which the $_{583}$KEKID$_{587}$ COP1-binding motif is com-

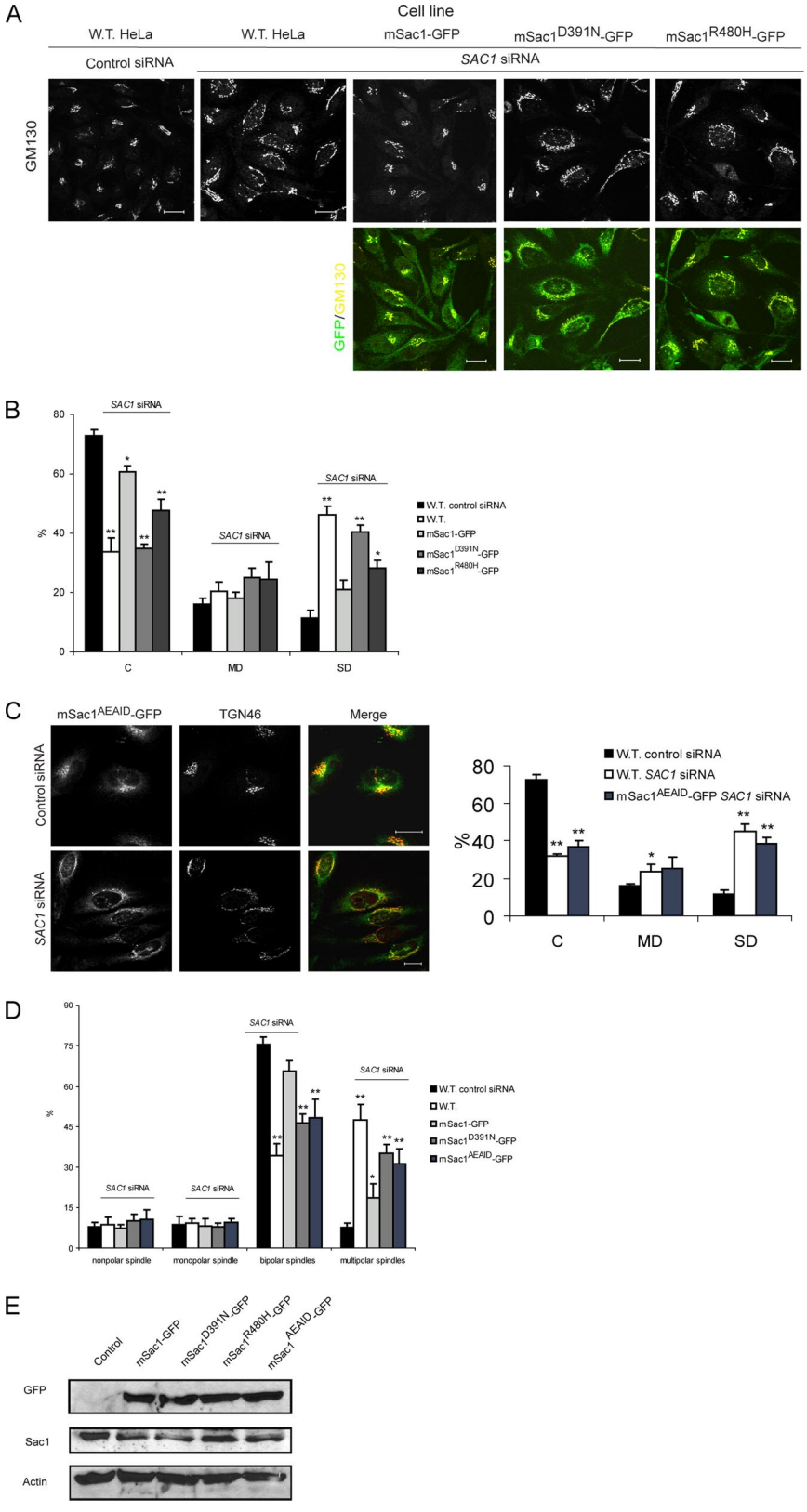

Figure 10. Functional properties of Sac1. (A) HeLa cell lines that express wild type mSac1-GFP, mSac1^{D391N}-GFP, or mSac1^{R480H}-GFP from a stably integrated lentiviral vector were challenged with control or *hSAC1* siRNAs and processed for immunofluorescence microscopy. Golgi are marked by GM130 (yellow), and mSac1-GFP and mutant variants are shown as green. Bar, 20 μm. (B) Golgi membranes of cells described in A were classified as compact (C), moderately dispersed (MD), or severely dispersed (SD). More than 300 cells were examined for Golgi morphology. Data are presented as mean values and standard deviations obtained from three independent experiments with >100 cells examined per experiment (*$p < 0.05$ and **$p < 0.001$). (C) HeLa cells expressing mSac1^{AEAID}–GFP from an integrated lentiviral vector were treated with control- or *hSAC1*-siRNAs and processed for immunofluorescence. More than 300 cells were examined for Golgi morphology. Data are presented as mean values and standard deviations obtained from three independent experiments with >100 cells examined per experiment (*$p < 0.01$ and **$p < 0.001$). Bar, 20 μm. (D) Sac1 phosphatase activity and coatomer binding and rescue of the spindle defects. siRNA experiments were performed with wild-type HeLa and lines expressing mSac1-GFP, mSac1^{D391N}-GFP, or mSac1^{AEAID}-GFP. Forty-eight hours after siRNA challenge, cells were fixed and spindle morphology was visualized by α-tubulin staining. Data are summed from three independent experiments, and >400 cells were examined from three independent transfections per experiment (*$p < 0.05$ and **$p < 0.001$). (E) HeLa cells expressing mSac1-GFP, mSac1^{D391N}-GFP, mSac1^{R480H}-GFP or mSac1^{AEAID}-GFP from an integrated lentiviral vector were processed for immunoblotting with anti-hSac1, anti-GFP, and anti-actin antibodies. HeLa cells with no GFP transgene served as controls.

promised, was ineffective in rescuing derangements in Golgi or spindle organization inflicted by hSac1 depletion (Figure 10, C and D). Nonfunctionality of mSac1^{D391N}-GFP and mSac1^{AEAID}-GFP in the complementation assay was not a trivial result. The biologically inactive mSac1^{D391N}-GFP and mSac1^{AEAID}-GFP, and the partially functional mSac1^{R480H}-GFP, all accumulated to steady-state levels similar to those measured for mSac1-GFP (Figure 10E).

Functional Distinction between Mammalian Sac1 and ARF Depletion

The coatomer binding requirement for hSac1 function is consistent with ER localization as an essential feature of hSac1 biological activity. Alternatively, it could indicate a role for hSac1 in biogenesis of COP1 vesicles. A COP1-centric model implies a critical involvement for hSac1 in ER retrieval pathways. Previous depletion studies with the Arf1 and Arf4 isoforms lend weight to this possibility (Volpicelli-Daley *et al*., 2005). Codepletion of Arf1 and Arf4 evokes Golgi dysmorphologies resembling the ones observed upon hSac1 depletion. To distinguish between these possibilities, two experiments were performed. First, we tested whether a soluble resident of the ER lumen (BiP), a protein actively retrieved from the Golgi by the KDEL receptor pathway (Bole *et al*., 1986; Lewis and Pelham, 1992; Orci *et al*., 1997), is inappropriately secreted in hSac1-depleted cell populations. This is expected if hSac1 is required for formation of COP1 vesicles that help retrieve BiP. No significant increase in extracellular BiP was detected in culture supernatants of hSac1-depleted cells relative to controls (data not shown).

Second, we adopted the approach of Volpicelli-Daley *et al*. (2005) and codepleted HeLa cells of both Arf1 and Arf4. As described previously, such codepletion results in wholesale release of the β-COP subunit of the coatomer complex from Golgi membranes and evokes dramatic dispersal and tubulation of Golgi membranes (Supplemental Figure S6). Although the Golgi dispersal phenotype is superficially similar to the effects seen upon hSac1 depletion, we note Golgi membranes retain coatomer under conditions of hSac1 insufficiency (see above). Moreover, neither individual depletion of Arf1 or Arf4 nor codepletion of both Arf1 and Arf4 had any effect on mitotic spindle organization in Arf-deficient cell populations (Supplemental Figure S6). The collective data indicate hSac1 deficiency interfaces with Golgi organization and mitotic spindle function in a manner that is not tightly linked to activity of the Arf/coatomer system. We conclude the functional requirement for the physical interaction between hSac1 and coatomer reflects the necessity of hSac1 to reside in the ER, rather than an hSac1 requirement for Arf/coatomer function.

DISCUSSION

Herein, we report a comprehensive analysis of mammalian Sac1 PIP phosphatase function. We demonstrate loss of Sac1 activity leads to preimplantation lethality in the mouse. Consistent with an essential housekeeping function for mammalian Sac1, hSac1 depletion is deleterious to the cell viability of immortalized human cell lines, and this morbidity is associated with inefficient progression though the G2/M phase of the cell cycle. From an intracellular perspective, Sac1 insufficiencies manifest themselves in specific derangements of Golgi membrane architecture that are apparent across all Golgi subcompartments, and in mitotic arrest. The pronounced mitotic arrest associated with hSac1 depletion is characterized by a highly elevated incidence of cells with ectopic mechanically active spindles. Finally, rescue studies establish that 1) the Golgi and mitotic spindle defects result from hSac1 insufficiency and not depletion of some other unintended target; 2) specific loss of Sac1 phosphatase activity is sufficient to evoke the Golgi membrane and mitotic spindle disorganization; and 3) competence for COPI-dependent recycling from the Golgi system back to the ER, represents an essential property for mammalian Sac1 function in vivo.

Sac1 and Golgi Membrane Architecture

An attractive mechanism for Golgi disorganization under conditions of hSac1 insufficiency is release of peripheral membrane proteins that regulate the architecture of this organelle. Given that catalytic activity of mammalian Sac1 is required for rescue of the Golgi dysmorphology phenotype, one attractive possibility is disorganization of the Golgi system is evoked by mislocalization of specific PIP-binding proteins. Such mislocalization could result from precocious accumulation of PtdIns-4-P pools in inappropriate membrane compartments (as demonstrated in *sac1*Δ yeast; Li *et al*., 2002). Marker localization experiments, however, do not report a significant redistribution of candidate PIP-binding proteins. No obvious mislocalization of Golgi-associated PtdIns-4-P-binding proteins was recorded in *hSAC1*-silenced cells. Thus, derangement of cellular PtdIns-4-P is either limited to a quantitatively minor pool that does not lead to a manifest redistribution of peripheral Golgi membrane proteins that bind PtdIns-4-P, or excess PtdIns-4-P is effectively sequestered by other high-affinity binding proteins. An alternative possibility is activities of other proteins that control Golgi structure and function (e.g., ARF) are compromised by hSac1 deficiencies. We find no evidence to support this view either. The lack of perturbation, by hSac1 insufficiency, of PtdIns-4-P-binding protein distribution, ARF pathway function, or PITPβ association with Golgi membranes is congruent with the transport competence of the disorganized Golgi system. This conclusion holds the caveat that all measurements of secretory pathway efficacy were conducted under conditions of reduced hSac1 function. All hSac1-insufficiency phenotypes are expected to be more extreme under conditions of Sac1 nullizygosity. It remains possible that a defect is imposed on membrane trafficking through and from the mammalian Golgi stack under authentic Sac1 null conditions.

Sac1 and Progression through the Cell Cycle

Preservation of trafficking competence for the disorganized Golgi membranes of hSac1-depleted cells suggests the morphological defect reflects compromise of some other layer of structural regulation for this organelle. In that regard, the mammalian Golgi complex is disassembled from its pericentriolar disposition by a highly regulated course of mitotic fragmentation involving mitogen-activated protein (MAP) kinase and polo-like kinase pathways (Nelson, 2000; Rossanese and Glick, 2001; Colanzi *et al*., 2003a,b; Ruan *et al*., 2004; Xie *et al*., 2004), and they are subsequently further vesiculated in a Cdc2-dependent manner (Lowe *et al*., 1998). The dispersed Golgi membranes in hSac1-depleted cells bear a superficial resemblance to those adopted by Golgi membranes during a normal course of mitosis. One interpretation of the data is that the Golgi dispersion phenotypes of hSac1-deprived cells reflect a defect in progression though the cell cycle, rather than a simple defect in Golgi organization per se.

hSac1-deficient cells are competent to enter mitosis, but they exhibit a high incidence of failure in properly organizing the mitotic spindle. These cells arrest in metaphase and present both condensed chromatin and multiple mechanically active spindles. The ectopic spindles are not the result of derangements in centrosome duplication. The acentriolar ectopic spindles nevertheless exert sufficient force to drive aberrant segregation of chromosomal material. Such defects in organization of mechanically active spindles likely result in chromosomal nondisjunction events (Wong and Stearns, 2003), thereby defining an attractive mechanism for why

mammalian cells deprived for Sac1 PIP phosphatase activity fail to efficiently progress though G2/M and die. Several aspects of the mitotic spindle phenotype recapitulate effects seen when Golgi-associated protein GRASP-65 expression is silenced in HeLa cells (Sütterlin *et al.*, 2005). One major distinction is that the multiple spindles of GRASP-65-deficient mitotic cells are not mechanically active (Sütterlin *et al.*, 2005). Consistent with this distinction, GRASP-65 levels are not reduced upon hSac1 deprivation (data not shown). Thus, the mitotic defects associated with hSac1- and GRASP-65 depletion derive from what are apparently distinct mechanisms.

The coincidence of Golgi and mitotic spindle structural defects in hSac1- and GRASP-65–deprived cells reinforces the intimate relationship between the Golgi apparatus and control of spindle dynamics in higher eukaryotes. In particular, these findings support conclusions that the Golgi apparatus and the centrosome are both spatially and functionally linked in mammalian cells (Sutterlin *et al.*, 2005; Kodani and Sutterlin, 2008; Lin *et al.*, 2007). Those various observations raise the possibility of a causal relationship between Golgi dysmorphology and the mitotic spindle defects that accompany hSac1 depletion. In that regard, recent work demonstrates TGN membranes have an intrinsic capability to nucleate MTs (Efimov *et al.*, 2007). Because the TGN seems enriched in PtdIns-4-P, this raises the possibility that excess PtdIns-4-P directly results in precocious nucleation of spindle poles. Alternatively, Golgi membrane and mitotic spindle organization may be confused in parallel by deranged PIP pools that accumulate when Sac1 activity in the ER is reduced below critical thresholds. Although we cannot yet distinguish between these possibilities, both concepts raise interesting possibilities regarding general principles for Sac1 function in mammalian cells. It is also worth emphasizing that Golgi disorganization does not inevitably lead to defects in spindle dynamics. Codepletion of Arf1 and Arf4 exerts major defects in Golgi morphology without deranging the organization of mitotic spindles.

A Role for Sac1 in Regulating Nuclear PIP Signaling?

Recent studies indicate Sac1 localization in mammalian cells is influenced by growth factor status. That is, under conditions of growth factor limitation, hSac1 is localized to Golgi membranes, whereas it redistributes to the ER upon growth factor resupply (Blagoveshchenskaya *et al.*, 2008). These data are consistent with hSac1 inhibiting membrane trafficking in cells experiencing growth factor distress, and hSac1 relocalization to the ER as release of the trafficking brake upon growth factor supplementation (Blagoveshchenskaya *et al.*, 2008). Yet, in yeast (Rivas *et al.*, 1999) and now in mammals, it is essential that Sac1 PIP phosphatase activity be localized to ER membranes for proper biological function. This is not consistent with simple models where ER-localized Sac1 represents some inactive pool poised for activation upon redistribution to the Golgi complex.

Why then is hSac1 residence in the ER of functional importance? It is presently accepted that PIPs are not generated in the ER and that no ER functions exhibit PIP dependence. This requirement is made all the more curious by the fact that ySac1 activity is, by all measure, dedicated to degradation of PtdIns-4-P generated specifically by the plasma membrane Stt4 PtdIns 4-OH kinase (Nemoto *et al.*, 2000; Foti *et al.*, 2001), although the possibility that plasma membrane/ER contact sites may represent sites of functional interface between these enzymes cannot yet be excluded (Routt *et al.*, 2005). What functional rationale underlies such a paradoxical circuit? One idea is that PIP phosphatases function primarily to degrade PIPs that occur in inappropriate compartments. The net effect of such a "mop-up" activity is to reinforce specific localization of PIP species so as to establish/maintain a "membrane PIP-code" that helps specify organelle identity. In our view, this simplistic model does not adequately account for cardinal properties of Sac1 PIP phosphatase function. We find no evidence for wholesale mislocalization of intracellular PIP-binding proteins in Sac1-deficient HeLa cells. Moreover, a Sac1 involvement in mop-up of mislocalized PIPs in ER membranes demands effective PIP channeling to the ER for degradation. If PIPs are rapidly mobilized between intracellular membranes in vivo, such as is the case for phosphatidylserine (Wu *et al.*, 2000; Wu and Voelker, 2004), why would cells choose an organelle with a large membrane surface (i.e., ER) for such duty? A large membrane area will only dilute unrestricted PIPs over its surface and reduce the efficiency with which Sac1 consumes PIP substrates.

In our view, the available data are more consistent with directed regulatory functions for Sac1 PIP phosphatases in the ER, rather than with menial PIP-mop-up duties. What might such regulatory functions be? We can only speculate at this point. However, the ER is contiguous with the outer nuclear envelope (Mattaj, 2004), and the nuclear matrix is a physiologically significant site of PIP signaling (Irvine, 2002; Cocco *et al.*, 2004; Manzoli *et al.*, 2005; Martelli *et al.*, 2005; Bunce *et al.*, 2006). In that regard, the nuclear PIP 3-OH kinase-C2β is activated during G2/M in human cells (Dobos *et al.*, 1993; Cappellini *et al.*, 2003; Visnjic *et al.*, 2003). The continuity of the nuclear envelope with ER suggests Sac1 PIP phosphatases may reside in the ER to regulate nuclear PIP signaling during the cell cycle. The derangements in spindle organization associated with Sac1-deficiencies are consistent such an involvement. To our knowledge, there are (as yet) no functional data to link PIPs to activity of any specific factor that participates in recruitment of γ-tubulin ring complex ring complexes to centrosomes, or to any other subunit of the spindle apparatus. Nonetheless, previous studies reported that the nuclear PtdIns decrease by >50%, and PtdIns-4-P and PtdIns-4,5-P_2 levels decrease by 66%, in S phase mammalian cells, even though bulk membrane PtdIns and PIPs do not fluctuate so (York and Majerus, 1994). These nuclear PIP dynamics are not only consistent with a role for PIPs in regulating nuclear functions in a cell cycle-dependent manner, but raise the question by what mechanisms are nuclear PIP levels depressed during S phase. One interesting possibility is a nuclear pool of the appropriate PIP phosphatases oversees such a regulation. A second possibility is that PtdIns-4-P (or some 3-OH phosphorylated PIP) is mobilized from the nuclear matrix/envelope to the ER and subsequently degraded by Sac1. Perhaps Sac1 deficiencies evoke derangements of nuclear PIPs, and these derangements contribute to the formation of ectopic spindle poles. Because the nuclear matrix seems incompetent for de novo PtdIns synthesis (Rubbini *et al.*, 1997; Martelli *et al.*, 2005), this scenario forecasts both exquisite control of PtdIns import into the nuclear matrix and regulated degradation of nuclear PIPs by enzymes other than phospholipases C. Moreover, given the physiological coupling between ySac1 and the Stt4 PtdIns 4-OH kinase in yeast, it is of interest to assess whether mammalian Sac1 also displays such a specific dedication to degradation of PIP produced by a specific PtdIns (or PIP) kinase and, if so, which PtdIns kinase.

In summary, we demonstrate the Sac1 PIP phosphatase executes essential housekeeping functions required for proper Golgi and mitotic spindle organization in mammals. We further show these essential functions require both PIP

phosphatase activity and proper COP1-dependent retrograde trafficking of these enzymes so that Sac1 can be efficiently retained in ER membranes. The cell cycle defects of Sac1-deficient cells forecast these enzymes as underappreciated, yet central integrators of PIP signaling in subcellular compartments not normally considered as centers for intracellular lipid signaling.

ACKNOWLEDGMENTS

We acknowledge our University of North Carolina (UNC) colleagues Kristina Ile and Carl Mousley for critical comments on the manuscript; Wendy Salmon for assistance with live cell imaging experiments; Peter Petrusz and Gail Grossman for advice in histochemical staining, Randy Thresher for assistance with blastocyst injections; Terry Magnuson, Yijing Chen, and Kim Kluckman for tutelage in mouse embryology; Hal Mekeel for training in electron microscopy; Liang Cai for lentiviral and PML vectors; and Jean Cook and Kathleen Nevis for help with FACS. Fluorescence imaging experiments were performed at the UNC Michael Hooker Microscopy Facility. We are grateful to Peter Mayinger (University of Oregon Health Sciences Center) for anti-Sac1 antibody and for communicating results before publication, to Sima Lev (Weizmann Institute) for the VSV-G tsO45 plasmid, to Neale Ridgway (Dalhousie) for OSBP and Orp9 antibodies, to Rick Kahn (Emory) for the *ARF1* and *ARF4* silencing plasmids, and to Jim Collawn and Elizabeth Sztul (University of Alabama Medical Center) for anti-transferrin antibodies and helpful discussion, respectively. Finally, we thank John York and Jim Otto (Duke) for helpful discussions and for help with PIP analyses. This work was supported by National Institutes of Health grant NS-37723 (to V.A.B.).

REFERENCES

Alb, J. G., Jr. *et al*. (2002). Genetic ablation of phosphatidylinositol transfer protein function in murine embryonic stem cells. Mol. Biol. Cell *13*, 739–754.

Blagoveshchenskaya, A., Cheong, F. Y., Rohde, H. M., Glover, G., Knödler, A., Nicolson, T., Boehmelt, G., and Mayinger, P. (2008). Integration of Golgi trafficking with growth factor signaling by the lipid phosphatase SAC1. J. Cell Biol. *180*, 803–812.

Bohil, A. B., Robertson, B. W., and Cheney, R. E. (2006). Myosin-X is a molecular motor that functions in filopodia formation. Proc. Natl. Acad. Sci. USA *103*, 12411–12416.

Bole, D. G., Hendershot, L. M., and Kearney, J. F. (1986). Posttranslational association of immunoglobulin heavy chain binding protein with nascent heavy chains in nonsecreting and secreting hybridomas. J. Cell Biol. *102*, 1558–1566.

Bunce, M. W., Bergendahl, K., and Anderson, R. A. (2006). Nuclear PI(4,5)P(2): a new place for an old signal. Biochim. Biophys. Acta *1761*, 560–569.

Cappellini, A., Tabellini, G., Zweyer, M., Bortul, R., Tazzari, P. L., Billi, A. M., Fala, F., Cocco, L., and Martelli, A. M. (2003). The phosphoinositide 3-kinase/Akt pathway regulates cell cycle progression of HL60 human leukemia cells though cytoplasmic relocalization of the cyclin-dependent kinase inhibitor p27(Kip1) and control of cyclin D1 expression. Leukemia *17*, 2157–2167.

Chen, J. L., Xu, W., and Stamnes, M. (2005). In vitro reconstitution of ARF-regulated cytoskeletal dynamics on Golgi membranes. Methods Enzymol. *404*, 345–358.

Cleves, A., McGee, T., and Bankaitis, V. (1991). Phospholipid transfer proteins: a biological debut. Trends Cell Biol. *1*, 30–34.

Cleves, A. E., Novick, P. J., and Bankaitis, V. A. (1989). Mutations in the SAC1 gene suppress defects in yeast Golgi and yeast actin function. J. Cell Biol. *109*, 2939–2950.

Cocco, L., Capitani, S., Maraldi, N. M., Martelli, A. M., Mazzotti, G., and Manzoli, F. A. (2004). Significance of nuclear phospholipase C signaling though type 1 IGF receptor. J. Endocrinol. Invest. *27*, 143–145.

Colanzi, A., Suetterlin, C., and Malhotra, V. (2003a). Cell-cycle-specific Golgi fragmentation: how and why? Curr. Opin. Cell Biol. *15*, 462–467.

Colanzi, A., Sutterlin, C., and Malhotra, V. (2003b). RAF1-activated MEK1 is found on the Golgi apparatus in late prophase and is required for Golgi complex fragmentation in mitosis. J. Cell Biol. *161*, 27–32.

Cremona, O. *et al*. (1999). Essential role of phosphoinositide metabolism in synaptic vesicle recycling. Cell *99*, 179–188.

Dobos, G. J., Wu, X. R., and Traynor-Kaplan, A. (1993). A product of phosphatidylinositol-3 kinase is elevated in dividing HT29 colonic epithelial cells. FEBS Lett. *324*, 143–146.

Duden, R., Griffith, G., Frank, R., Argos, P., and Kreis, T. E. (1991). beta-COP, a 110 kD protein associated with non-clathrin-coated vesicles and the Golgi complex, shows homology to beta-adaptin. Cell *64*, 649–665.

Efimov, A. *et al*. (2007). Asymmetric CLASP-dependent nucleation of noncentrosomal MTs at the trans-Golgi network. Dev. Cell *12*, 917–930.

Foti, M., Audhya, A., and Emr, S. D. (2001). Sac1 lipid phosphatase and Stt4 PtdIns-4-kinase regulate a pool of PtdIns(4)P pool that functions in control of the actin cytoskeleton and vacuole morphology. Mol. Biol. Cell *12*, 2396–2411.

Fruman, D. A., Meyers, R. E., and Cantley, L. C. (1998). Phosphoinositide kinases. Annu. Rev. Biochem. *67*, 481–507.

Godi, A., Di Campli, A., Konstantakopoulos, A., Di Tullio, G., Alessi, D. R., Kular, G. S., Daniele, T., Marra, P., Lucocq, J. M., and De Matteis, M. A. (2004). FAPPs control Golgi-to-cell-surface membrane traffic by binding to ARF and PtdIns(4)P. Nat. Cell Biol. *6*, 393–404.

Guo, S., Stolz, L. E., Lemrow, S. M., and York, J. D. (1999). SAC1-like domains of yeast SAC1, INP52, and INP53 and of human synaptojanin encode polyphosphoinositide phosphatases. J. Biol. Chem. *274*, 12990–12995.

Hama, H., Schnieders, E. A., Thorner, J., Takemoto, J. Y., and DeWald, D. B. (1999). Direct involvement of phosphatidylinositol 4-phosphate in secretion in the yeast *Saccharomyces cerevisiae*. J. Biol. Chem. *274*, 34294–34300.

Hinchcliffe, E. H., and Sluder, G. (2001). "It takes two to tango": understanding how centrosome duplication is regulated throughout the cell cycle. Genes Dev. *15*, 1167–1181.

Hughes, W. E., Woscholski, R., Cooke, F. T., Patrick, R. S., Dove, S. K., McDonald, N. Q., and Parker, P. J. (2000). SAC1 encodes a regulated lipid phosphoinositide phosphatase, defects in which can be suppressed by the homologous Inp52p and Inp53p phosphatases. J. Biol. Chem. *275*, 801–818.

Irvine, R. F. (2002). Nuclear lipid signaling. Sci. STKE *2002*, RE13.

Kearns, B. G., McGee, T. P., Mayinger, P., Gedvilaite, A., Phillips, S. E., Kagiwada, S., and Bankaitis, V. A. (1997). Essential role for diacylglycerol in protein transport from the yeast Golgi complex. Nature *387*, 101–105.

Khodjakov, A., and Rieder, C. L. (1999). The sudden recruitment of gamma-tubulin to the centrosome at the onset of mitosis and its dynamic exchange throughout the cell cycle, do not require MTs. J. Cell Biol. *146*, 585–596.

Kodani, A., and Sutterlin, C. (2008). The Golgi protein GM130 regulates centrosome morphology and function. Mol. Biol. Cell *19*, 745–753.

Konrad, G., Schlecker, T., Faulhammer, F., and Mayinger, P. (2002). Retention of the yeast Sac1p phosphatase in the endoplasmic reticulum causes distinct changes in cellular phosphoinositide levels and stimulates microsomal ATP transport. J. Biol. Chem. *277*, 10547–10554.

Lessmann, E., Ngo, M., Leitges, M., Minguet, S., Ridgway, N. D., and Huber, M. (2007). Oxysterol-binding protein-related protein (ORP) 9 is a PDK-2 substrate and regulates Akt phosphorylation. Cell Signal. *19*, 384–392.

Lewis, M. J., and Pelham, H. R. (1992). Ligand-induced redistribution of a human KDEL receptor from the Golgi complex to the endoplasmic reticulum. Cell *68*, 353–364.

Li, X., Rivas, M. P., Fang, M., Marchena, J., Mehotra, B., Chaudhary, A., Feng, L., Prestwich, G. D., and Bankaitis, V. A. (2002). Analysis of oxysterol binding protein homologue Kes1p function in regulation of Sec14p-dependent protein transport from the yeast Golgi complex. J. Cell Biol. *157*, 63–77.

Lin, X., Liu, C. C., Gao, Q., Zhang, X., Wu, G., and Lee, W. H. (2007). RINT-1 serves as a tumor suppressor and maintains Golgi dynamics and centrosome integrity for cell survival. Mol. Cell Biol. *27*, 4905–4916.

Litvak, V., Dahan, N., Ramachandran, S., Sabanay, H., and Lev, S. (2005). Maintenance of the diacylglycerol level in the Golgi apparatus by the Nir2 protein is critical for Golgi secretory function. Nat. Cell Biol. *7*, 225–234.

Lowe, M., Rabouille, C., Nakamura, N., Watson, R., Jackman, M., Jamsa, E., Rahman, D., Pappin, D. J., and Warren, G. (1998). Cdc2 kinase directly phosphorylates the cis-Golgi matrix protein GM130 and is required for Golgi fragmentation in mitosis. Cell *94*, 783–793.

Maehama, T., Taylor, G. S., and Dixon, J. E. (2001). PTEN and myotubularin: novel phosphoinositide phosphatases. Annu. Rev. Biochem. *70*, 247–279.

Majerus, P. W. (1997). Inositol phosphatases and kinases in cell signaling. FASEB J. *11*, A1297.

Manzoli, L., Martelli, A. M., Billi, A. M., Faenza, I., Fiume, R., and Cocco, L. (2005). Nuclear phospholipase C: involvement in signal transduction. Prog. Lipid Res. *44*, 185–206.

Martelli, A. M., Fiume, R., Faenza, I., Tabellini, G., Evangelista, C., Bortul, R., Follo, M. Y., Fala, F., and Cocco, L. (2005). Nuclear phosphoinositide specific phospholipase C (PI-PLC)-beta *1*, a central intermediary in nuclear lipid-dependent signal transduction. Histol. Histopathol. *20*, 1251–1260.

Mattaj, I. W. (2004). Sorting out the nuclear envelope from the endoplasmic reticulum. Nat. Rev. Mol. Cell Biol. *5*, 65–69.

Moudjou, M., Bordes, N., Paintrand, M., and Bornens, M. (1996). gamma-Tubulin in mammalian cells: the centrosomal and the cytosolic forms. J. Cell Sci. *109*, 875–887.

Nagy, A., Gertsenstein, M., Vintersten, K., and Behringer, R. (2003). Manipulating the Mouse Embryo: A Laboratory Manual, 3rd ed., Cold Spring Harbor, NY: Cold Spring Harbor Laboratory Press.

Nelson, W. J. (2000). W(h)ither the Golgi during mitosis? J. Cell Biol. *149*, 243–248.

Nemoto, Y., Kearns, B. G., Wenk, M. R., Chen, H., Mori, K., Alb, J. G., Jr., De Camilli, P., and Bankaitis, V. A. (2000). Functional characterization of a mammalian Sac1 and mutants exhibiting substrate-specific defects in phosphoinositide phosphatase activity. J. Biol. Chem. *275*, 34293–34305.

Novick, P., Osmond, B. C., and Botstein, D. (1989). Suppressors of yeast actin mutations. Genetics *121*, 659–674.

Oprins, A., Duden, R., Kreis, T. E., Geuze, H. J., and Slot, J. W. (1993). beta-COP localizes mainly to the cis-Golgi side in exocrine pancreas. J. Cell Biol. *121*, 49–59.

Orci, L., Stamnes, M., Ravazzola, M., Amherdt, M., Perrelet, A., Sollner, T. H., and Rothman, J. E. (1997). Bidirectional transport by distinct populations of COPI-coated vesicles. Cell *90*, 335–349.

Phillips, S. E., Sha, B., Topalof, L., Xie, Z., Alb, J. G., Klenchin, V. A., Swigart, P., Cockcroft, S., Martin, T. F., Luo, M., and Bankaitis, V. A. (1999). Yeast Sec14p deficient in phosphatidylinositol transfer activity is functional in vivo. Mol. Cell *4*, 187–197.

Phillips, S. E., Ile, K., Boukhelifa, M., Huijbregts, R.P.H., and Bankaitis, V. A. (2006). Specific and nonspecific membrane binding determinants cooperate in targeting phosphatidylinositol transfer protein β-isoform to the murine *trans*-Golgi network. Mol. Biol. Cell *17*, 2498–2512.

Presley, J. F., Cole, N. B., Schoer, T. A., Hirschberg, K., Zaal, K. J., and Lippincott-Schwartz, J. (1997). ER-to-Golgi transport visualized in living cells. Nature *389*, 81–85.

Rivas, M. P., Kearns, B. G., Xie, Z., Guo, S., Sekar, M. C., Hosaka, K., Kagiwada, S., York, J. D., and Bankaitis, V. A. (1999). Pleiotropic alterations in lipid metabolism in yeast sac1 mutants: relationship to "bypass Sec14p" and inositol auxotrophy. Mol. Biol. Cell *10*, 2235–2250.

Rohde, H. M., Cheong, F. Y., Konrad, G., Paiha, K., Mayinger, P., and Boehmelt, G. (2003). The human phosphatidylinositol phosphatase SAC1 interacts with the coatomer I complex. J. Biol. Chem. *278*, 52689–52699.

Rossanese, O. W., and Glick, B. S. (2001). Deconstructing Golgi inheritance. Traffic *2*, 589–596.

Routt, S. M., Ryan, M. M., Tyeryar, K., Rizzieri, K., Roumanie, O., Brennwald, P. J., and Bankaitis, V. A. (2005). Nonclassical PITPs activate phospholipase D via an Stt4p-dependent pathway and modulate function of late stages of the secretory pathway in vegetative yeast cells. Traffic *6*, 1157–1172.

Ruan, Q., Wang, Q., Xie, S., Fang, Y., Darzynkiewicz, Z., Guan, K., Jhanwar-Uniyal, M., and Dai, W. (2004). Polo-like kinase 3 is Golgi localized and involved in regulating Golgi fragmentation during the cell cycle. Exp. Cell Res. *294*, 51–59.

Rubbini, S., Cocco, L., Manzoli, L., Lutterman, J., Billi, A. M., Matteucci, A., and Wirtz, K.W.A. (1997). Biochem. Biophys. Res. Commun. *230*, 302–305.

Rubinson, D. A. *et al*. (2003). A lentivirus-based system to functionally silence genes in primary mammalian cells, stem cells and transgenic mice by RNA interference. Nat. Genet. *33*, 401–406.

Salisbury, J. L., Suino, K. M., Busby, R., and Springett, M. (2002). Centrin-2 is required for centriole duplication in mammalian cells. Curr. Biol. *12*, 1287–1292.

Scales, S. J., Pepperkok, R., and Kreis, T. E. (1997). Visualization of ER-to-Golgi transport in living cells reveals a sequential mode of action for COPII and COPI. Cell *90*, 1137–1148.

Srinivasan, S., Seaman, M., Nemoto, Y., Daniell, L., Suchy, S. F., Emr, S., De Camilli, P., and Nussbaum, R. (1997). Disruption of three phosphatidylinositol-polyphosphate 5-phosphatase genes from *Saccharomyces cerevisiae* results in pleiotropic abnormalities of vacuole morphology, cell shape, and osmo-homeostasis. Eur. J. Cell Biol. *74*, 350–360.

Stolz, L. E., Kuo, W. J., Longchamps, J., Sekhon, M. K., and York, J. D. (1998). INP51, a yeast inositol polyphosphate 5-phosphatase required for phosphatidylinositol 4,5-bisphosphate homeostasis and whose absence confers a cold-resistant phenotype. J. Biol. Chem. *273*, 11852–11861.

Strahl, T., and Thorner, J. (2007). Synthesis and function of membrane phosphoinositides in budding yeast, *Saccharomyces cerevisiae*. Biochim. Biophys. Acta *1771*, 353–404.

Sütterlin, C., Polishchuk, R., Pecot, M., and Malhotra, V. (2005). The Golgi-associated protein GRASP65 regulates spindle dynamics and is essential for cell division. Mol. Biol. Cell *16*, 3211–3222.

Tahirovic, S., Schorr, M., and Mayinger, P. (2005). Regulation of intracellular phosphatidylinositol-4-phosphate by the Sac1 lipid phosphatase. Traffic *6*, 116–130.

Visnjic, D., Curic, J., Crljen, V., Batinic, D., Volinia, S., and Banfic, H. (2003). Nuclear phosphoinositide 3-kinase C2beta activation during G2/M phase of the cell cycle in HL-60 cells. Biochim. Biophys. Acta *1631*, 61–71.

Volpicelli-Daley, L. A., Li, Y., Zhang, C. J., and Kahn, R. A. (2005). Isoform-selective effects of the depletion of ADP-ribosylation factors 1–5 on membrane traffic. Mol. Biol. Cell *16*, 4495–4508.

Walch-Solimena, C., and Novick, P. (1999). The yeast phosphatidylinositol-4-OH kinase pik1 regulates secretion at the Golgi. Nat. Cell Biol. *1*, 523–525.

Wenk, M. R., and De Camilli, P. (2004). Protein-lipid interactions and phosphoinositide metabolism in membrane traffic: insights from vesicle recycling in nerve terminals. Proc. Natl. Acad. Sci. USA *101*, 8262–8269.

Whitters, E. A., Cleves, A. E., McGee, T. P., Skinner, H. B., and Bankaitis, V. A. (1993). SAC1p is an integral membrane protein that influences the cellular requirement for phospholipid transfer protein function and inositol in yeast. J. Cell Biol. *122*, 79–94.

Wishart, M. J., and Dixon, J. E. (2002). PTEN and myotubularin phosphatases: from 3-phosphoinositide dephosphorylation to disease. Trends Cell Biol. *12*, 579–585.

Wishart, M. J., Taylor, G. S., Slama, J. T., and Dixon, J. E. (2001). PTEN and myotubularin phosphoinositide phosphatases: bringing bioinformatics to the lab bench. Curr. Opin. Cell Biol. *13*, 172–181.

Wong, C., and Stearns, T. (2003). Centrosome number is controlled by a centrosome-intrinsic block to reduplication. Nat. Cell Biol. *5*, 539–544.

Wu, W.-I., Routt, S., Bankaitis, V. A., and Voelker, D. (2000). A new gene involved in transport-dependent metabolism of phosphatidylserine, *PSTB2/PDR17*, shares sequence similarity with the gene encoding the phosphatidylinositol/phosphatidylcholine transfer protein, Sec14p. J. Biol. Chem. *275*, 14446–14456.

Wu, W.-I., and Voelker, D. (2004). Reconstitution of phosphatidylserine transport from chemically defined donor membranes to phosphatidylserine decarboxylase 2 implicates specific lipid domains in the process. J. Biol. Chem. *279*, 6635–6642.

Wyles, J. P., and Ridgway, N. D. (2004). VAMP-associated protein-A regulates partitioning of oxysterol-binding protein-related protein-9 between the endoplasmic reticulum and Golgi apparatus. Exp. Cell Res. *297*, 533–547.

Xie, S., Wang, Q., Ruan, Q., Liu, T., Jhanwar-Uniyal, M., Guan, K., and Dai, W. (2004). MEK1-induced Golgi dynamics during cell cycle progression is partly mediated by Polo-like kinase-3. Oncogene *23*, 3822–3829.

Xie, Z., Fang, M., Rivas, M. P., Faulkner, A. J., Sternweis, P. C., Engebrecht, J. A., and Bankaitis, V. A. (1998). Phospholipase D activity is required for suppression of yeast phosphatidylinositol transfer protein defects. Proc. Natl. Acad. Sci. USA *95*, 12346–12351.

York, J. D., and Majerus, P. W. (1994). Nuclear phosphatidylinositols decrease during S-phase of the cell cycle in HeLa cells. J. Biol. Chem. *269*, 7847–7850.